12-2018

Experimental Investigation of a Green Hybrid Thruster Using a Moderately Enriched Compressed Air as the Oxidizer

Marc Anthony Bulcher
Utah State University

EXPERIMENTAL INVESTIGATION OF A GREEN HYBRID THRUSTER USING A MODERATELY ENRICHED COMPRESSED AIR AS THE OXIDIZER

by

Marc Anthony Bulcher

A thesis submitted in partial fulfillment
of the requirements for the degree

of

MASTER OF SCIENCE

in

Aerospace Engineering

Approved:

Stephen A. Whitmore, Ph.D. Major Professor	David Geller, Ph.D. Committee Member
Geordie Richards, Ph.D. Committee Member	Richard S. Inouye, Ph.D. School of Graduate Studies

UTAH STATE UNIVERSITY
Logan, Utah

2018

ABSTRACT

Experimental Investigation of a Green Hybrid Thruster using a Moderately Enriched Compressed Air as the Oxidizer

by

Marc Anthony Bulcher, Master of Science

Utah State University, 2018

Major Professor: Stephen A. Whitmore, Ph.D.
Department: Mechanical and Aerospace Engineering

The majority of space missions launched to date have relied on propulsion systems that employ hydrazine as their primary propellant. Hydrazine is highly toxic and potentially explosive, and the special procedures necessary for safe handling and operations have become increasingly cost prohibitive, especially for the emerging commercial spacecraft industry. Both NASA and the DOD are actively seeking safer and greener replacements for this propellant. In response to this challenge, the Propulsion Research Laboratory at Utah State University has developed a viable "green" alternative hydrid rocket sysem that is based on 3D printed thermoplastics as rocket fuels.

Traditionally, hybrid rockets have never been seriously considered as viable for in-space propulsion due to the lack of a reliable on-demand ignition system. However, when certain 3D printed thermoplastics are subjected to a high-voltage, low-wattage charge, electrostatic arcing along the surface vaporizes a small amount of material. When the vaporized fuel comes into contact with an oxidizer, combustion is seeded and produces immediate and reliable motor ignition. Best performing among the tested 3D printed thermoplastic materials is acrylonitrile butadiene styrene (ABS).

Through the course of several research programs, this physical property has been developed into a simple, low-wattage, on demand hybrid ignition system with a moderately high Technology Readiness Level. Motivated by this enabling discovery, USU has recently begun testing very small-scale, low mass flow hybrid rockets for space propulsion applications. These inherently safe, "green" propulsion technologies are being targeted as potential low-cost drop-in replacements for many hydrazine-based systems. Direct on demand ignition has been demonstrated using ABS and gaseous oxygen (GOX) for multiple motor configurations with thrust levels varying from less than 5 N to greater than 900 N. Nitrous Oxide and 90% Hydrogen peroxide have also been demonstrated to be effective as oxidizers for this system. GOX has clearly demonstrated the best overall system performance, with specific impulse values more than 20% higher than mono-propellant hydrazine.

Unfortunately, GOX at low pressures is rather low density compared to hydrazine, and in order to ensure a high level of volumetric efficiency, GOX must be stored at high pressures, often greater than 3000 psig. GOX stored at high pressures creates a high level of fire danger, and precision cleaning and maintenance of spacecraft components is required. The use of GOX-rated aerospace components are also required for safe operation. These specialized requirements can lead to cost-prohibitive system designs. However, most materials designed for use with standard air delivery can be adapted for use with enriched air – up to 40% oxygen concentration – with little or no hardware modifications. Precision cleaning, hardware logging, and tracking of flow path components is not required. Thus, if the green thruster system designed for GOX usage can be demonstrated to perform effectively using enriched air, these exists the potential for a significant reduction in operating costs.

This thesis investigates the feasibility of replacing GOX with compressed air containing oxygen levels up to 40%. At 3000 psi, the resulting O_2 partial pressures for these mixtures varies from 630 to 1200 psig; levels well below upper limits allowed for nearly all industrial, commercial aviation, and medical applications. Analytical and ground test results are presented, and are supported by data collected from a single hard-vacuum sub-orbital flight test. Arc-ignition feasibility using compressed air is demonstrated.

(96 pages)

PUBLIC ABSTRACT

Experimental Investigation of a Green Hybrid Thruster using a Moderately Enriched Compressed Air as the Oxidizer

Marc Anthony Bulcher

A hybrid rocket is a propulsion system that uses propellants in two different phases, typically a solid fuel inside the combustion chamber and a separate gaseous or liquid oxidizer stored in a tank. Hybrid rockets are an area of research interest because of their low explosive risk, inexpensive components, and high degree of reliability. In the Propulsion Research Laboratory at Utah State University, pure oxygen is among the top choice for hybrid rocket oxidizers due to its low cost and ease of storage. When paired with a solid fuel known as ABS (acrylonitrile butadiene styrene) plastic, specific impulse values exceed 200 seconds at one atmosphere. This metric outperforms hydrazine, which is a propellant standard for in-space propulsion that exhibits high vapor toxicity and explosive hazards. However, due to the low density of oxygen, propulsion applications require storage pressures up to 3000 psig. At this high pressure, the use of oxygen can present a fire hazard. As a result, this thesis investigates the feasibility of replacing oxygen with a moderately enriched compressed air containing oxygen levels up to 40%, while maintaining performance metrics equal to or above hydrazine. To demonstrate the performance of moderately enriched air as a hybrid rocket oxidizer, comparisons to tests using pure oxygen are presented.

ACKNOWLEDGMENTS

I want to thank Dr. Stephen Whitmore for allowing me the opportunity to work in his lab. I also want to thank him for trusting me with the NASA sub-orbital flight project, it was an honor to work that to completion. Many thanks to my colleagues for their input and help with part fabrication. Lastly, I thank my wife for her sacrifice by working and supporting me throughout my graduate school education, none of this would have been possible without her love and (financial) support.

Marc Anthony

CONTENTS

Page

LIST OF TABLES

LIST OF FIGURES

NOTATION

A_1	Venturi Inlet Area
A_2	Venturi Throat Area
A_t	Nozzle Throat Area
A_p	Fuel Port Area
a	Regression Rate Scaling Factor
C_d	Injector Discharge Coefficient
C_f	Skin Friction Coefficient
c_p	Specific Heat
G_{ox}	Fuel Port Mass Flux
H_{vap}	Enthalpy of Vaporization
L	Fuel Grain Length
Pr	Prandtl Number
M_{fuel}	Fuel Mass
$\dot{m}_{ox}$	Oxidizer Mass Flow Rate
$\dot{m}_{fuel}$	Fuel Mass Flow Rate
$\dot{m}_{total}$	Total Exit Mass Flow Rate
n	Regression Rate Burn Exponent
O/F	Oxidizer-to-Fuel Ratio
P_0	Chamber Pressure
P_1	Venturi Inlet Pressure
P_2	Venturi Throat Pressure
$\dot{Q}_{convection}$	Convection Heat Flux
$\dot{Q}_{fuelvap}$	Heat Flux Required for Fuel Vaporization
$\dot{Q}_{radiation}$	Radiation Heat Flux

$\dot{r}$	Fuel Regression Rate
r_p	Fuel Port Radius
S_t	Stanton Number
T_{flame}	Combustion Flame Temperature
$T_{fuelsurface}$	Fuel Surface Temperature
T	Oxidizer Temperature
$T_{0_{CEA}}$	CEA Combustion Temperature
T_{0a}	Actual Chamber Temperature
U_x	Fuel Port Axial Velocity
$V_{consumed}$	Fuel Volume Consumed
α	Absorbtivity
β	Blowing Coefficient
ρ_f	Fuel Density
γ	Ratio of Specific Heats
η	Combustion Efficiency
μ	Dynamic Viscosity
τ	Skin Friction Coefficient
σ	Stefan-Boltzmann Constant
ϵ	Emissivity

ACRONYMS

ABS	Acrylonitrile Butadiene Styrene
CEA	Chemical Equilibrium with Applications
EAN	Enriched Air Nitrox
FDM	Fused Deposition Modeling
GOX	Gaseous Oxygen
HTPB	Hydroxyl Terminated Polybutadiene
HVPS	High Voltage Power Supply
LOX	Liquid Oxygen
MMH	Mono Methyl Hydrazine
MSFC	Marshall Space Flight Center
NASA	National Aeronautics and Space Administration
NI	National Instruments
NTO	Nitrogen Tetroxide
PPU	Power Processing Unit
PRL	Propulsion Research Laboratory
TRL	Technology Readiness Level
UDMH	Unsymmetrical Di-Methyl Hydrazine
USAF	United States Air Force
USIP	Undergraduate Student Instrument Project
USU	Utah State University

CHAPTER 1

INTRODUCTION

1.1 Early History of Hybrid Rockets

The earliest known hybrid rocket to be successfully tested was designed by a small group of Soviet engineers. Led by Mikhail Tikhonravov and Sergei Korolev, the group known as *GIRD*, which in the Russian acronym means the Group for the Study of Reactive Motion, launched a hybrid rocket in August, 1933 [1]. The rocket was coined $O9$, which consisted of a jellied gasoline fuel and a liquid oxygen (LOX) oxidizer. Weighing just 42 pounds, *O9* rose to a height of approximately 1300 feet. It was the successful launch of *O9* that caught the attention of the Soviet military. A few years after the creation of GIRD, the group disbanded; however, it was Tikhonravov and Korolev that went on to head other projects such as the launch of Sputnik. A few years after the launch of *O9*, surrounding institutions began their own testing of hybrid rockets with fuels such as graphite and coal. In 1937, researchers at I. G. Farben developed and tested their own Coal/Nitrous Oxide hybrid rocket attaining thrust levels up to 2200 lbf. However, due to the large heat of sublimation of carbon, the motors fuel regression rate was negligible, inducing motor inefficiencies. The same problems impacted the Graphite/LOX hybrid rocket built in the late 1930's by H. Oberth in Germany [2].

It was not until the mid 1940's that the Pacific Rocket Society out of California began experimenting with their own series of hybrid rockets with varying solid fuels and LOX as the oxidizer. Their first, and perhaps most notable hybrid rocket, used a one pound Douglas Fir fuel grain. The Douglas Fir/LOX hybrid rocket ascended to a height of 650 feet before the oxygen tank exploded after only 2.5 seconds of burn time [3]. The Pacific Rocket Society continued to develop and test other fuels, and in 1953 experienced great success when using a rubber polymer known as $Thiokol$ as fuel. They deemed this $Thiokol/LOX$

hybrid rocket the $XDF-23$ and made a debut in the Popular Mechanics magazine in April of 1954 [4]. The acronym XDF was coined after their first launch of the Douglas Fir hybrid rocket meaning *Experimental Douglas Fir*. The number following the acronym signified the current iteration of the hybrid rocket. The success of the Pacific Rocket Society's hybrid rocket experimentation likely acted as a catalyst in other scientific communities putting their time and money into research and development of hybrid rockets.

Around this same time, General Electric initiated their own in-depth investigation into hybrid rocket research and development. They began testing hybrid rockets with a polyethylene based fuel and hydrogen peroxide as the oxidizer [2]. General Electric made several significant observations during their testing that helped the scientific community to further understand hybrid rocket physics. One observation was that cracks in the fuel did not have any influence on the chamber pressure during the burn, as it does in solid rockets. Another observation was that the chamber pressure seemed proportional to the mass flow rate of oxidizer. From these observation, it could be deduced that hybrid rocket physics are fundamentally different than the physics that govern solid rocket behavior.

It was not until 1963 when a sufficiently complete analysis of hybrid rockets was published by Marxman and Gilbert [5]. They outlined the basics of hybrid rocket combustion and discovered that fuel regression is dominated by diffusion as compared to chemical kinetics in solid rockets.

1.2 Background

All too often, the assumption is made that solid and hybrids rockets can be modeled using the same ballistics. Had hybrid rocket research ended with the investigation made by General Electric in the 1950's, their observations alone would prove otherwise. Solid rockets are highly pressure coupled, meaning any increase in fuel surface area due to unforeseen cracks in the grain or propellant structure instability can exponentially increase chamber pressure to the point of catastrophic breakdown. Solid rockets are, however, the most volumetrically efficient propulsion system. Though, solids arguably lack the greatest perk of both hybrid and either monopropellant or bipropellant liquid propulsion systems because

they can only burn one time. Monoprop refers to a propellant containing both an oxidizing agent and a fuel, whereas biprop refers to a propellant with separated fuel and oxidizer. Once started, a solid rocket cannot turn off until all the propellant has been consumed. Both liquid and hybrid rockets have the ability to start, stop, and restart. However, biprop liquid rockets are extremely sophisticated in their design; requiring turbo-pumps for propellant flow and pyrophoric chemicals for the ignition sequence to avoid damaging the combustion chamber upon startup. If the liquid rocket is of the monoprop type, volume inefficient and inert mass components such as catalyst beds, heaters, and top-pressurant tanks are commonly required. These mass components are deemed 'inert' because on their own, do not add to the total delivered impulse.

Hybrid rockets are of particular research interest because they are inherently safer than other rocket designs and do not require the convolution of monoprop or biprop liquid rockets. The idea behind hybrid rockets is to store the solid fuel inside the combustion chamber, and the oxidizer as a liquid or gas in a separate pressure vessel. This produces a propulsion system less susceptible to explosions than traditional solid and liquid propellant rockets. To a degree, hybrid rockets combine many of the advantages of solid and liquid propellant rocket motors.

Like solid rockets, hybrid rockets are easily stored and have a long shelf life if the oxidizer is non-cryogenic. Identical in theory, hybrid and liquid rockets share the ability to be throttled, stopped, and restarted on demand. However, the manner in which these restart capabilities are executed differ in both complexity and cost. Standard methods exist for ignition sequences of liquid systems, whereas reliable on-demand ignition systems for hybrid rockets have not been widely researched. As a result, hybrid rockets have never been seriously considered for alternative in-space propulsion.

While researching 3-D printable plastics as alternatives to legacy thermosetting polymer materials like hydroxyl-terminated polybutadiene (HTPB), the Propulsion Research Laboratory (PRL) at Utah State University (USU) discovered that acrylonitrile butadiene styrene (ABS) serves as an efficient alternative to HTPB. ABS plastic is a common thermo-

plastic polymer known for its structural properties and widely used in the automotive trim industry, plumbing, and Lego bricks [6]. The production of ABS and HTPB are different; HTPB fuel grains are made from a labor intensive process involving mixing, casting, and curing. In direct comparison, ABS plastic can be extruded or manufactured through fused deposition modeling (FDM). In FDM, a thermoplastic filament is unwound from a coil, similar to a fishing rod reel, that supplies material to a heated extrusion nozzle. The nozzle melts the plastic to achieve extrusion. The position of the nozzle is computer controlled in three dimensions using various robotic components. FDM production of ABS plastic allows for the development of complex fuel port geometries, a feat difficult to attain through HTPB casts. An environmentally advantageous benefit of ABS plastic is that its recyclable, able to be reshaped and wound into plastic filaments to be used again. Once an HTPB fuel grain is cast, the fuel cannot be recycled. However, HTPB remains the most widely used hybrid rocket fuel due to its well known chemical composition and combustion properties. Further, Whitmore et al. [7] analytically and experimentally compared HTPB and ABS as hybrid rocket fuels. Their results led to the viability of using 3-D printed ABS plastic as a hybrid rocket fuel in place of HTPB due to its competitive performance, and inexpensive and ease of manufacturing. This discovery led to the development of a unique on-demand patented arc ignition technology for hybrid rockets [8].

In this concept, electrical breakdown properties of 3D printed ABS are exploited to develop a power efficient system that can be started and stopped, on demand, with a high degree of reliability. This is accomplished through an ignition system power processing unit (PPU), which is based on the UltraVolt line of high voltage power supplies (HVPS). Two electrodes are embedded into the top face of the fuel grain. Wires are then routed from the electrodes to small gaps located on the impingement shelves in the pre-combustion chamber of the fuel grain. The wires are insulated by printed quarter-circular slots that insert into the electrode wire gaps with ABS cement as the binder. The conducting paths terminate facing each other, in line with the pre-combustion port surface, and exposed to the interior of the combustion chamber. The HVPS provides the inductive spark necessary

to vaporize the ABS fuel to seed combustion. When an electrostatic potential is placed across the electrodes, electricity flows through a pre-existing surface arc-track, resulting in vaporization of the 3D printed ABS fuel. The charge produces localized arcing between the printed material layers, and the dissipated energy results in a material glass-transition from crystalline to amorphous. The amorphous layer is highly conductive, allowing the electrical arcs to cause a surface char-layer with the result being a surface arc-track. However, the arc-track must be set by dusting the surface of the pre-combustion chamber with graphite powder. The application of graphite decreases the impedance across the ABS surface between the electrode ends allowing successful arc tracking. Once a surface arc path has been set, graphite dusting is no longer required. Through several testing campaigns of a baseline 38mm diameter motor involving hundreds of successful burns, experience with this ignition system has demonstrated that ignition can be reliably achieved using as little as 4.1 watts [9].

The baseline hybrid rocket with a 2.1:1 expansion ratio nozzle, when tested at ambient pressure conditions achieved a thrust level slightly less than 20 N with a specific impulse (I_{sp}) of up to 201 seconds. When the same motor was tested in a vacuum chamber, a thrust level of approximately 26 N with an I_{sp} of 220 seconds was achieved. When the nozzle was expanded to a near optimal 9.5:1 expansion ratio, the respective thrust and I_{sp} improved to nearly 31 N and 280 seconds [9]. The baseline motor I_{sp} is 20-25% higher than can be achieved by mono-propellant hydrazine [10].

1.3 Research Motivation - Hydrazine

The current state-of-the-art propellant for small to medium spacecraft is hydrazine; a highly toxic, explosive, and cost prohibitive clear liquid. At standard temperature and pressure, hydrazine will vaporize completely due to its high vapor pressure. Vaporized hydrazine induces additional handling risks, such as inhalation and when contact is made between hydrazine and organic tissue, severe burns or permanently disabling injuries will result. Under certain conditions, hydrazine has potential to spontaneously decompose or detonate; though, a sufficient heat source or oxidizing agent must be present. These in-

herently dangerous features require that when handling hydrazine, personnel must wear a self-contained Hazmat suit due to the toxicity and instability of the propellant. The National Fire Prevention Agency (NFPA) diamond classification in Fig. 1.1. summarizes the associated hazards of using hydrazine as a propellant.

Diamond	Hazard	Value	Description
	Health	4	Can be lethal
	Flammability	4	Burns readily. Rapidly or completely vaporizes at atmospheric pressure and normal ambient temperature.
	Instability	3	Capable of detonation or explosive decomposition or explosive reaction but requires a strong initiating source or must be heated under confinement before intitiation.
	Special		

Fig. 1.1: NFPA Diamond Classification for Hydrazine

These hazards adversely affect the true cost of hydrazine, which lie in the tightly controlled transport, storage, servicing, and cleanup of accidental releases. These growing regulatory burdens have led to the increasingly cost prohibitive nature of servicing payloads using hydrazine-based propulsion systems. Operations involving toxic propellants on spacecraft are severely restricted. Any system modifications made on or near launch day or exchange of equipment requires the removal of hydrazine from the spacecraft, all while the work area is cleared and only trained personnel in Hazmat suits can remain on-site. These hydrazine-related launch procedures incur increased operational costs [11]. Though, due to its high degree of long-term reliability as a propellant, companies continue to use hydrazine. The going rate of hydrazine is often hidden, though SpaceX procured Ultra-Pure hydrazine for their Iridium NEXT satellites at a cost of $85.00/pound [12]. It is likely this price accounts only for the hydrazine and ignores the additional cost of storage, transport, and filling procedures. Though hydrazine has many inherent downfalls such as volatility and cost, it remains widely used on small spacecraft as a means of propulsion and attitude

control for three main reasons: 1) proven reliability 2) indeterminate shelf life and 3) it is the only well researched and proven in-space propellant at this time.

Hydrazine propellants exist in several varying forms such as anhydrous hydrazine, mono-methyl hydrazine (MMH), and unsymmetrical di-methyl hydrazine (UDMH). Each derivative of hydrazine exhibits slightly modified performance metrics, e.g., the range of stable operating temperatures, heat of decomposition, or application optimization [10]. Hydrazine can be used in monoprop or biprop configurations, each with their own performance and complexity trade-off. Monopropellant hydrazine systems require the addition of a costly catalyst bed with embedded heaters, and a pressurant tank and a pump for propellant flow. In this monoprop configuration, hydrazine does not burn when passing through the heated catalyst bed, but rather dissociates, expands, and releases a large amount of heat. The vacuum I_{sp} for monopropellant hydrazine systems do not exceed 225s, far less than the USU baseline 38mm ABS/GOX hybrid rocket system. When MMH or UDMH are used in a biprop configuration with either nitrogen tetroxide (NTO) or LOX as oxidizers, the maximum theoretical range of I_{sp} is 277-303 seconds [10]. However, LOX would never be used in small-spacecraft operations because of storage requirements, and NTO produces poisonous gases leading to further restrictive applications of bipropellant hydrazine. With the current state of propulsion technology, the only proven non-hazardous propulsion alternative to hydrazine, and available for small ride-share payloads, is based on low-performing cold-gas systems and power inefficient electrical propulsion.

The restrictive handling precautions surrounding hydrazine generally do not favor its use as a propellant for secondary payloads. Secondary payloads that rely on toxic or hazardous propellants present a potential risk to the primary payload and are generally excluded under most launch rules. Thus, because the majority of commercial and academic small spacecraft rely on ride-share or secondary payload launch opportunities, development of a non-toxic or "green" and cost-effective replacement for hydrazine-based propulsion systems is necessary for the emerging commercial spacecraft industry. A non-toxic "green" propellant is loosely defined as a substance whose only qualifying characteristic is being less

hazardous than hydrazine [13], though not environmentally friendly as the term implies.

1.4 Green Propellant Status

Currently, efforts are underway by NASA's Green Propellant Infusion Mission (GPIM) in furthering the development and characterization of two "green" propellants. The first propellant is called AF-M315E, based on hydroxylammonium nitrate, was originally developed by the United States Air Force (USAF) at the Edwards Air Force Base in California in 2001 [14]. AF-M315E offers greater performance than monopropellant hydrazine, able to produce an I_{sp} of 257 seconds, and is nearly 50% more dense [15]. These fundamental propellant metrics advantageously affect both the required propellant and volume of the tank in comparison to an identical hydrazine system. Another benefit of AF-M315E is its long-term storage thermal management system, unable to freeze according to Aerojet Rocketdyne, nulling the common requirement of maintaining a minimum propellant temperature. However, all AF-M315E systems still have embedded tank heaters to bring the propellant up to temperature during the catalyst bed pre-heat sequence. This is a requirement for hydrazine-based propulsion systems, where the tank must be maintained at approximately 20 °C. This is a power inefficient requirement for small to medium spacecraft due to their limited photovoltaic power production.. The overall safety requirements for handling AF-M315E is far less hazardous than traditional hydrazine systems, especially in direct comparison to the range requirements in handling both propellants. These range requirements are partially highlighted by the following examples and how they impact the hazard classification of AF-M315E.

The greater viscosity of AF-M315E compared to hydrazine decreases the chances of tank leakage and to its benefit, is considered non-toxic if a leak occurs. According to the Kennedy Space Center range safety personnel, AF-M315E has a hazard severity classification of "critical" based on the Standard Practice for System Safety MIL-STD-882E. In a direct comparison, if a hydrazine system were to leak, the same safety organization would deem it a hazard rating of "catastrophic." In addition to its decreased risk of both leaking and hazard classification, the AF-M315E thrusters are unable to fire if the catalyst bed is

not first preheated. These noted advantages of AF-M315E help to further reduce its cost, required power, and total mass of the thruster, while maintaining a hydrazine-equivalent system reliability. Thermal characteristics of AF-M315E compared to hydrazine require a higher catalyst bed preheat temperature, thus a larger load on the embedded photovoltaic cell is required than a conventional hydrazine system. Though, supporting documentation for AF-M315E based systems will declare that the decreased minimum storage temperature and smaller solenoid valves offsets the power requirement for a higher catalyst temperature.

The second propellant is known as LMP-103S, based on ammonium dinitramide, and was originally developed in Sweden. According to NASA Marshall Space Flight Center (MSFC), LMP-103S and AF-M315E perform similarly to hydrazine, each with their own trade-offs and safety advantages. Rather than testing both in an effort to narrow the selection to only one propellant, NASA's Charles Pierce, manager of MSFC's Spacecraft Propulsion Systems Branch said "NASA needs to have flexibility in the types of thrusters and propellant systems it has to meet a variety of mission needs. One type of propellant might work best for one type of mission while another is better suited for a different mission. It's important that we have choices as we go green."

Although NASA is working with AF-M315E and LMP-103S in an effort to go green, the safety requirements in handling both propellants differ by a single severity classification. When the word "green" is used to describe these propellants, the word often loses its value because it becomes construed to take on the meaning of "not hydrazine." This is an inherent fallacy in researching, developing, and discussing actual propellants that would be green by definition, benign in nature, and safe to handle without incurring financially draining safety equipment. The safety commission at KSC deeming AF-M315E a hazard class one step below hydrazine, while claiming it as a green propellant is a falsehood highlighted in Fig. 1.2. Exposure to AF-M315E per its hazard rating of "critical," according to MIL-STD-882E, could result in one of the following: permanent partial disability, injuries or occupational illness that may result in hospitalization of at least three personnel, reversible significant environmental impact, or monetary loss equal to or exceeding $1M but less than $10M.

SEVERITY CATEGORIES		
Description	**Severity Category**	**Mishap Result Criteria**
Catastrophic	**1**	Could result in one or more of the following: death, permanent total disability, irreversible significant environmental impact, or monetary loss equal to or exceeding $10M.
Critical	**2**	Could result in one or more of the following: permanent partial disability,injuries or occupational illness that may result in hospitalization of at least three personnel, reversible significant environmental impact, or monetary loss equal to or exceeding $1M but less than $10M.
Marginal	**3**	Could result in one or more of the following: injury or occupational illness resulting in one or more lost work day(s), reversible moderate environmental impact, or monetary loss equal to or exceeding $100K but less than $1M.
Negligible	**4**	Could result in one or more of the following: injury or occupational illness not resulting in a lost work day, minimal environmental impact, or monetary loss less than $100K.

Fig. 1.2: Department of Defense, Standard Practice, System Safety

By the loosely defined and often misinterpreted definition of a "green" propellant, AF-M315E cannot fall under its category because it is capable of causing severe physiological damage to the human body. Due to the many hazards associated with the use of hydrazine, AF-M315E, and LMP-103S, USU embarked on a research endeavor to design a non-toxic green propellant that can be handled with minimal risks.

1.5 USU Green Hybrid Rocket

Through the course of several research programs, the ABS/GOX hybrid rocket at USU has been developed into a simple, low wattage, on demand hybrid rocket system with a moderately high Technology Readiness Level (TRL) of 5 since its first tests in 2012. In comparison, it was not until 2011 that AF-M315E ascended to TRL5 and currently, NASA's GPIM claims a TRL7+. In four fewer years, USU's PRL developed a propulsion system yielding a 10% increase in I_{sp} over a green propellant developed by massive government-funded organizations. Direct on demand ignition has been demonstrated using ABS and gaseous oxygen (GOX) for multiple motor configurations with thrust levels varying from less than 5 N to greater than 900 N [16]. Figure 1.3 shows some of the scales of hybrid rocket fuels that have been successfully designed, fabricated, integrated, and test fired using this additive manufacturing and arc-ignition technology.

Fig. 1.3: Scalable 3D Printed ABS Fuel Grains

Each of the pictured motors uses identical technologies with the only tangible differences being the scale of the motor mold lines. Reliable on-demand ignition of a flight weight 38-mm diameter, 25 N thruster system has also been demonstrated during both ambient and soft vacuum operation using GOX and ABS as propellants [9]. Ambient tests of the 38mm small-scale motor, produced specific impulse values of up to 210 seconds with a 2.1:1 nozzle expansion ratio. The same motor when tested in a soft vacuum environment – approximately 0.15 atmospheres – with an optimized 9.5:1 expansion ratio nozzle produced an average I_{sp} of 280 seconds. When this performance is extrapolated to hard vacuum conditions, the projected I_{sp} exceeds 300 seconds. Although other high-density oxidizers including N_2O [17] and 90% H_2O_2 [18] have also been successfully demonstrated using the arc-ignition technology, a significant majority of the USU development tests have used GOX as the primary oxidizer due to the relative ease of management, low cost, and high performance.

Motivated by this promising green hybrid rocket, USU has recently begun testing very small scale, low mass flow hybrid rockets for space propulsion applications. These

inherently safe, green propulsion technologies are being shaped as potential low-cost drop-in replacements for many hydrazine-based propulsion systems. The system to be further developed and tested maintains consistent restart capability and the compact form factor of a hydrazine system, while improving significantly on safety, environmental sustainability, performance, power consumption, and cost of materials and operation. The development and testing of this flight weight system, along with the results from early development testing proves the ability of an additively manufactured fuel grain to be used as a drop-in replacement for hydrazine-based propulsion systems on small spacecraft.

The use of GOX in these small scale hybrid rockets is a step in the right direction over the use of hydrazine; however, due to the relatively low specific gravity of GOX, propulsion applications demand storage pressures up to 3000 psig. At these high pressures GOX presents a fire hazard that is not generally accepted by the rideshare community. As a fire-risk mitigation, this study investigates the feasibility of replacing GOX with compressed air containing oxygen levels up to 40%. At 3000 psi the resulting oxygen partial pressures for these mixtures varies from 630 to 1200 psig; levels well below upper limits allowed for nearly all industrial, commercial aviation, and medical applications. Analytical and ground test results will be presented, and supported by data collected from a single hard-vacuum sub-orbital flight test.

CHAPTER 2

HYBRID ROCKET THEORY

2.1 Regression Modeling and Comparisons

The physics that describe hybrid rocket combustion are fundamentally different than those that govern solid rocket motors. In solid rockets, the fuel regression rate is governed by what is known as Saint Robert's Law, shown by Eq. (2.1).

$$\dot{r} = aP_0^{n'} \tag{2.1}$$

In Saint Robert's Law, P_0 is the chamber pressure and a and n are empirically derived constants, where a scales the total regression rate and n is the pressure exponent. From this regression rate formulation, it becomes clear that with changes in chamber pressure and a given pressure exponent, the regression rate can fluctuate significantly and for this reason is said to be pressure coupled. Pressure coupling can become hazardous in the event of a sudden chamber pressure jump, which can occur if the propellant grain surface area grows unevenly due to surface fissures. However, if the propellant grain is within its design shelf life, the chance of deformities within the grain structure are unlikely. In total, solid rocket fuel regression is proportional to the chamber pressure and the chemical makeup of the propellant; whereas, hybrid rocket fuel regression cannot be modeled with with the same equation because they exhibit little pressure coupling. In comparison, the fuel regression rate in hybrid a rocket is directly proportional to the mass flux through the fuel grain port, as shown by Eq. (2.2).

$$\dot{r} = aG_{ox}^{n} \tag{2.2}$$

In this equation, a and n are empirically derived constants for a given fuel and oxidizer combination and G_{ox} refers to the oxidizer mass flux, and for the remainder of this paper will be presented in units of $g/cm^2 - s$. The fuel regression rate demonstrated by hybrid rockets is less than solid rocket motors, exhibiting values under 0.3 cm/s. Over the burn lifetime of an ABS/GOX hybrid rocket, observed regression rates typically fall in at under 0.28 cm/s [16], and decrease with time as the fuel port opens.

Originally, in 1963, Gilbert and Marxman published the first hybrid rocket ballistics model outlining the basics of fuel regression. Their accomplishment in hybrid rocket theory relied heavily on schlieren images published by R. J. Muzzy [19]. Schlieren photography is the process where light from a single source shines through some medium, for example butane from a lighter, which sits in front of a spherical or concave mirror. The reflective surface returns the incoming light to a camera, which sits at the focal point. The returned light is often too bright, so a knife can be used to block approximately half of the light returning to the camera. Based on the variations in the index of refraction caused by changes in density in the fluid medium, light fluctuations normally invisible to the human eye become visible. It was from this film technology and the experiments performed by R. J. Muzzy, that aided Gilbert and Marxman in deriving their hybrid rocket ballistics model. Their discovery led to the realization that hybrid rocket combustion is a function of oxidizer diffusion into the flame zone combustion layer between the outward blowing vaporized solid fuel and the axially flowing oxidizer. This fundamental hybrid rocket ballistics model is depicted below in Fig. 2.1.

The boundary layer lines are over exaggerated in Fig. 2.1; however, it gives insight into the combustion process within a hybrid rocket. Depicted in the figure is the solid fuel grain, the total combustion velocity profile U_x, oxidizer region, fuel and oxidizer mixture region, and the vaporized fuel region. The injector sprays the oxidizer into the combustion chamber, where it begins to mix with the vaporized solid fuel. In theory, this combustion process sounds similar to a traditional bi-propellant system. The primary differing factor being that hybrid rockets experience fuel regression rates corresponding to the rate of incoming

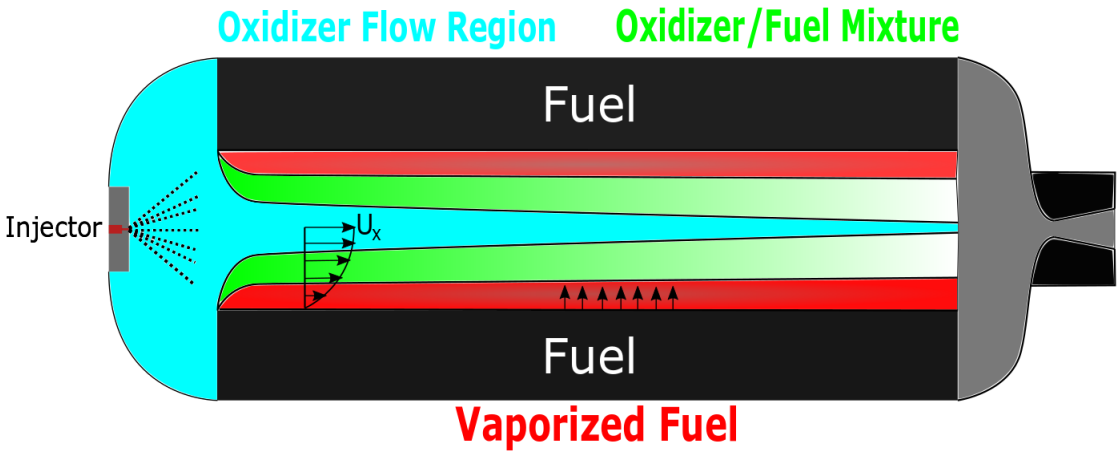

Fig. 2.1: Inkscape model of hybrid rocket combustion highlighting the various regions within the fuel port and the central boundary layer

injected oxidizer. This means that the rate at which fuel is consumed within the port of a hybrid rocket is inherently linked to the oxidizer flux. A dominant facet surrounding hybrid fuel regression is that it cannot be accurately predicted because of interactions between boundary layer thickness, fuel geometry, and oxidizer mass flux. These background fuel regression related features change as the fuel port opens up over the duration of the burn. Compared to solid rocket models, an accurate and comprehensive model of hybrid rocket combustion does not exist to reliably predict the fuel regression rate.

Figure 2.1 will be used as a free body diagram to setup the steady state equations that describe the fuel regression rate in hybrid rockets. After a brief derivation, the conclusion to the next section will contain the fuel regression model used to predict the hybrid rocket performance investigated in this thesis.

2.2 Hybrid Rocket Fuel Regression Model

This section contains the derivation and implemented fuel regression rate model used to predict hybrid rocket performance. The content in this section relies predominantly on the material found in sources [16], [20], [21].

The original Marxman model only accounts for the mass flux of oxidizer, which for fuel-lean burns is a reliable assumption; however, when modeling low mass flux hybrid rockets,

both oxidizer and fuel flux rates must be taken into account. At oxidizer-to-fuel (O/F) ratios below approximately four, a total port mass flux model should be used to account for the fractional increase in fuel flow. Additional research has been conducted to modify the classical Marxman relation to account for fuel rich scenarios, which may include an additional mode of heat transfer. The hybrid rocket fuel regression rate derivation begins by performing an enthalpy balance at the surface of the solid fuel grain. During steady state combustion a phase change occurs in that the solid fuel becomes gaseous and mixes with the injected oxidizer. This can be seen in Fig. 2.1 from the arrows pointing radially outward toward the center of the fuel port. The heat transfer modes are both convective and radiative, the influence of each term relying on motor scale and fuel-oxidizer chemistry. For the sake of this investigation, radiation heat transfer is included to account for the low mass flux of oxidizer. The energy balance of this process is shown in Eq. (2.3).

$$\dot{Q}_{fuel\ vap} = \dot{Q}_{convection} + \dot{Q}_{radiation} \tag{2.3}$$

These terms can be expanded and expressed into more useful terms using definitions associated with heat transfer. The term on the left becomes

$$\dot{Q}_{fuel\ vap} = mH_{vap} = \rho_f \dot{r} H_{vap} \tag{2.4}$$

where m is the mass, H_{vap} is the enthalpy of vaporization, ρ_f is the fuel density, and $\dot{r}$ is the regression rate. The convection term is expanded using the Stanton number, a dimensionless number relating the ratio of heat transferred to a fluid to the thermal capacity of the fluid.

$$\dot{Q}_{convection} = h\Delta T = S_t \rho U_x c_p \Delta T = S_t \rho U_x \Delta H \tag{2.5}$$

where S_t is the Stanton number, U_x is the axial port velocity, and ΔH is the flame-fuel change in enthalpy. The radiation term becomes

$$\dot{Q}_{radiation} = \sigma(\epsilon T_{flame}^4 - \alpha T_{fuel\ surface}^4) \tag{2.6}$$

where σ is the Stefan-Boltzmann constant, ϵ is the radiative emissivity, and α is the radiative absorbtivity. From hereon, the temperatures will be referred to as T_f and T_s for the flame and fuel surface respectively.

Combining Eqs. (2.4-2.6), the total heat flux at the fuel surface becomes

$$\rho_f \dot{r} H_{vap} = S_t \rho_f U_x \Delta H + \sigma(\epsilon T_f^4 - \alpha T_s^4) \tag{2.7}$$

In this equation, many of the terms are readily available such as the density of the fuel ρ_f, the fuel latent heat of vaporization H_{vap}, change in enthalpy across the flame-fuel surface ΔH, the Stefan Boltzmann constant σ, and the temperature of both the flame and fuel. The emissivity ϵ and absorbtivity α are not constants and can vary as the fuel regresses. Understanding of the radiation terms in small mass-flux hybrid rockets is not understood at the time of this document. The Stanton number in Eq. (2.7) does little to describe the physics of the fuel regression, and as it stands cannot be used without aid of the Chilton-Colburn Analogy (Reynolds Analogy). The Reynolds analogy is an empirical result that relates the skin friction coefficient C_f to the turbulent heat transfer and will not be discussed in further detail. The Reynolds analogy is shown below under the assumption that the Prandtl number is not unity.

$$S_t = \frac{C_f}{2Pr^{2/3}} \tag{2.8}$$

In this equation, the Prandtl number can be calculated using NASA's Chemical Equilibrium with Applications (CEA) program, though the skin friction coefficient still needs more work for it to consist of readily available parameters. Whitmore, et. al., model the skin friction coefficient by applying the Blasius formula for turbulent wall shear stress and substitute in the Schoenherr-Schlicting model for the turbulent boundary layer thickness. This relationship is shown in Eq. (2.9).

$$C_f = \frac{\tau}{\left(\frac{\rho U_x x}{\mu}\right)^{1-n}} \tag{2.9}$$

The exponent containing n in this equation is traditionally valued at 4/5 according to the original Marxman derivation. However, for the sake of this derivation, the exponent will remain as a changeable value. In addition to the axially flowing oxidizer that affects the local skin friction coefficient, so to does the radially outflowing vaporized fuel. This can be taken into account through the *Blowing* coefficient, which is the ratio of the shearing force due the outflow of fuel and the skin friction. The Boardman model equates the blowing coefficient to the ratio of the flame-fuel enthalpy to the fuel enthalpy of vaporization [21]. The skin friction coefficient is modified by the following equation:

$$C_B = \frac{1.27 C_f}{\beta^{0.77}} \tag{2.10}$$

where β is the blowing coefficient defined as the ratio of the flame-fuel change in enthalpy to the fuel enthalpy of vaporization.

Eq. (2.9) is a function of x, the length of the fuel port, and therefore must be averaged across the total length of the port. The mean skin friction coefficient as a function of the port length is shown in Eq. (2.11).

$$C_f = \frac{\tau}{n}\left(\rho U_x \frac{L}{\mu}\right)^{n-1} \tag{2.11}$$

Substituting Eq. (2.11) into Eq. (2.8) gives

$$S_t = \frac{\tau}{2nPr^{2/3}}\left(\rho U_x \frac{L}{\mu}\right)^{n-1} \tag{2.12}$$

Taking this result, making sure to account for the C_B term and plugging it into the enthalpy balance in Eq. (2.7) and solving for $\dot{r}$ gives:

$$\dot{r} = \frac{0.635\tau}{n\rho_f Pr^{2/3}\beta^{0.77}}\frac{\Delta H}{H_{vap}}\left(\frac{L}{\mu}\right)^{n-1} G_{ox}^{n} + \frac{\sigma(\epsilon T_f^4 - \alpha T_s^4)}{\rho_f H_{vap}} \tag{2.13}$$

This equation summarizes the fuel regression rate model used to predict the performance of the hybrid rocket. Due to the nature of the energy deficient oxidizer used throughout this study, several terms that can generally be assumed as constants are left in their native form for convenient manipulation. This was done because the interaction between the chosen oxidizers and fuel have never been examined. Due to the mass-flux dependent nature of hybrid rockets it was assumed that the wall shear stress τ and burn exponent n would need to be iterated upon to attempt a match between experiment and model. This assumption was made due to the fact that, at 40% concentration O_2, the enthalpy of combustion is small compared to that of pure GOX. At this low energy level, if combustion were to seed, the wall shear stress would have to be large if the flow rate of fuel remained similar to higher energy oxidizer burns. National Instruments (NI) LabVIEW was used as the programming language to implement the hybrid rocket model. Model predictions such as thrust, chamber pressure, and specific impulse from the hybrid rocket model will be discussed later in this thesis. The description of the implementation, however, is not important for the understanding of the material to be presented.

CHAPTER 3

EXPERIMENT SETUP

This chapter outlines and explains the experimental test setup. Along with the explanation is a summary containing motor geometry and instrumentation. Two modes of experimentation took place throughout this testing campaign. Each will be discussed and presented in detail.

3.1 Undergraduate Student Instrumentation Project - Phase 1 Setup

Two test pallets were designed to aid this thesis investigation: one for repetitive in-lab evaluation of a single motor configuration and the other for the NASA Undergraduate Student Instrument Project (USIP), which consisted of simultaneous dual ignition. The NASA USIP was awarded to USU to fly a prototype set of small-scale ABS hybrid thrusters to an apogee altitude of 100 miles aboard a Terrier Malemute Sounding Rocket. The rocket launched in March of 2018 from the test range at the NASA Wallops Flight Facility. The test platform spent more than 200 seconds above the 100 km "Von-Karman line in a hard vacuum environment. The experiment featured a set of two 6 N thrusters, with each performing multiple restarts. Figure 3.1 shows the completed USIP payload, featuring dual oxidizer tanks, twin 38mm hybrid rockets, and an electronics bay on the top deck. The thrusters were designed to be in a self-nulling configuration sharing the same flow path, hence simultaneous ignition occurred. This was done to aid in the prevention of moments that could affect NASA's payload. This experiment setup produced the data for the lowest O_2 concentration for this thesis at approximately 40% by volume, deemed Enriched Air Nitrox (EAN40). Data will also be presented from the sub-orbital flight test.

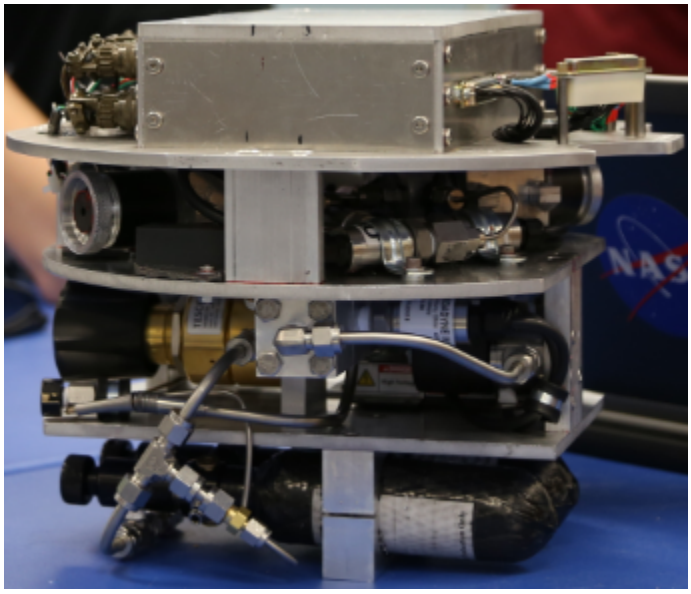

Fig. 3.1: Self-Nulling Hybrid Rocket USIP Payload

The primary goal of this thesis is to present data from hybrid rocket burns using an oxidizer with diminishing concentrations of O_2 and very low mass flux levels. The interest in this topic originally arose throughout the design of the USIP payload. As per NASA safety requirements, pressure vessels containing GOX were eventually barred from flight unless USU precision cleaned flow path equipment and procured space grade oxygen rated valves and tanks, which would have gone far beyond budget. The meaning behind this management decision was that pure oxygen at high pressures could lead to catastrophic breakdowns proving to be hazardous to the success of the mission. NASA was not wrong to stand by their decision because highly compressed oxygen can create a high level of fire danger.

In October of 2017, less than six months from launch, EAN40 was successfully demonstrated in the PRL. The choice was officially made to switch from GOX to EAN40. However, high pressure tanks were still an integral piece of the design and Range Safety required a two leak inhibit design. Two leak inhibit means that if one piece of hardware were to fail, no negative outcome would arise. This is deemed a single-fault tolerant design. To meet this Range Safety requirement, two solenoid valves were installed along the flow path to act

as mechanical inhibits. The complete plumbing diagram is shown below in Fig. 3.2 along with a description of the payload transducers and flow components.

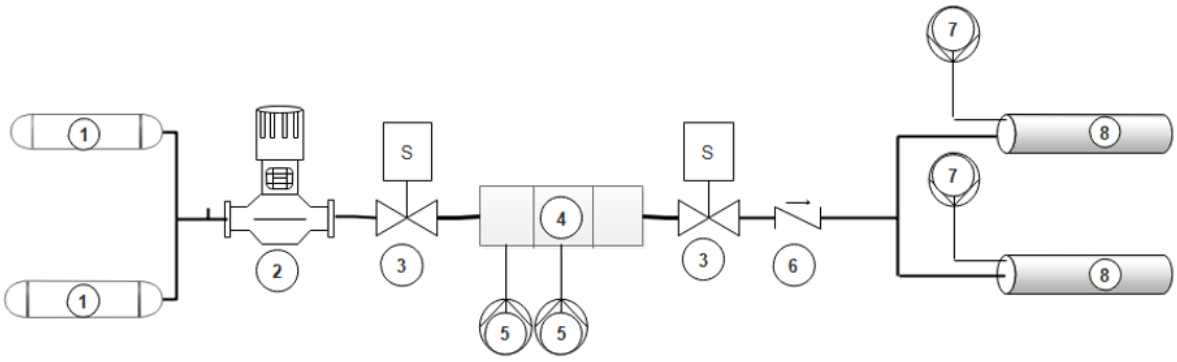

1	First Strike HPA Tank, 3000 psig, 13 cu. In. each, Tri-Label UN ISO approved
2	Panel-Mount High-Pressure Regulating Valve, 3500 psig inlet, 0-500 psig outlet, McMaster 3811T11
3	High-Pressure Compact Actuated On/Off Valve, 520 psig max pressure, McMaster 48325K443
4	Custom venturi flow meter - 6061 T6 Aluminum – Sufficient Safety Factor
5	Omega PX309-500GV
6	Corrosion-Resistant Backflow-Prevention Valve, 580 psig max pressure, McMaster8605T14
7	Omega PX309-150GV
8	38mm hybrid motors, high temperature aluminum case, nozzle, and injector cap

Fig. 3.2: Plumbing Diagram of the USIP Payload Design

The instrumentation used to measure the performance of these dual hybrid rockets consisted that of only pressure measurements. Venturi-based flow rates were measured with inlet and throat pressure transducers and each thrust chamber had its own independent pressure transducer. In addition to the pressure measurements, a thermocouple was installed aft the venturi to measure the temperature of oxidizer. This was done as a backup to independent temperature measurements; however, flow rates vary little with standard temperature fluctuations seen throughout the standard day. Due to volume constraints and the use of commercial off the shelf components, installing a thrust based load cell was not feasible. In addition, a load cell would have done little to express thruster performance due to the fact that ideally, equal and opposite forces would have been exerted upon each side. This would have output a zero measurement to the post-test file and would contribute little, if anything to the thruster assessment.

3.2 Undergraduate Student Instrumentation Project - Phase 2 Testing

The USIP payload testing took place in the USU PRL in the Industrial Science building room 101. The payload, previously shown in Fig. 3.1, was hung from a clevis-turnbuckle to allow a greater degree of freedom to observe any motor inconsistencies during burns. Shown in Fig. 3.3 is the dual thruster assembly on top of a tray of 36-3D printed fuel grains with a quarter for scale. It took approximately 58 fuel grains to sufficiently evaluate and qualify the ignition and steady state burn characteristics of EAN40.

The test procedure began by weighing the ABS fuel grains before assembling and installing the thrusters. Before hanging the payload for testing, the oxidizer tanks were filled with GOX to 1200 psi and then topped off with Nitrogen to 3000 psi, which led to an approximate O_2 molar concentration of 40%. The error in the mixture ratio primarily involved the resolution of the gages used to fill the tanks. A filling procedure designed for the NASA USIP safety management is included in the Appendix.

Once the payload was hung from the test bay, the 15-pin power and 37-pin telemetry cables were connected. To simulate the NASA interface as closely as possible, a custom LabVIEW VI control code was written to control the Ground Support Equipment (GSE) and the Timer Event Redundant (TER) pins in the 15-pin power cable. The GSE line gave power to the system, though without power to the TER line, the system could not initiate any firing sequence. This functionality allowed the payload to remain in stand-by mode until USU's 30-second testing window opened approximately 255 seconds into flight. The control VI front panel is shown in Fig. 3.4. The eight circular boolean displays in the upper part of Fig. 3.4 were to mimic visual system status that would be received during the NASA launch. The four waveform graphs were analog input channels used to monitor each motors real time ignition voltage and chamber pressure. The control panel shown is setup to monitor the chamber and the venturi flow pressures, though choices were available in which data was desired for situational awareness.

The hot fire tests were initiated by flipping the GSE-1 switch and waiting 30-seconds for the on-board computer to boot. Once the USIP payload was ready for testing, the

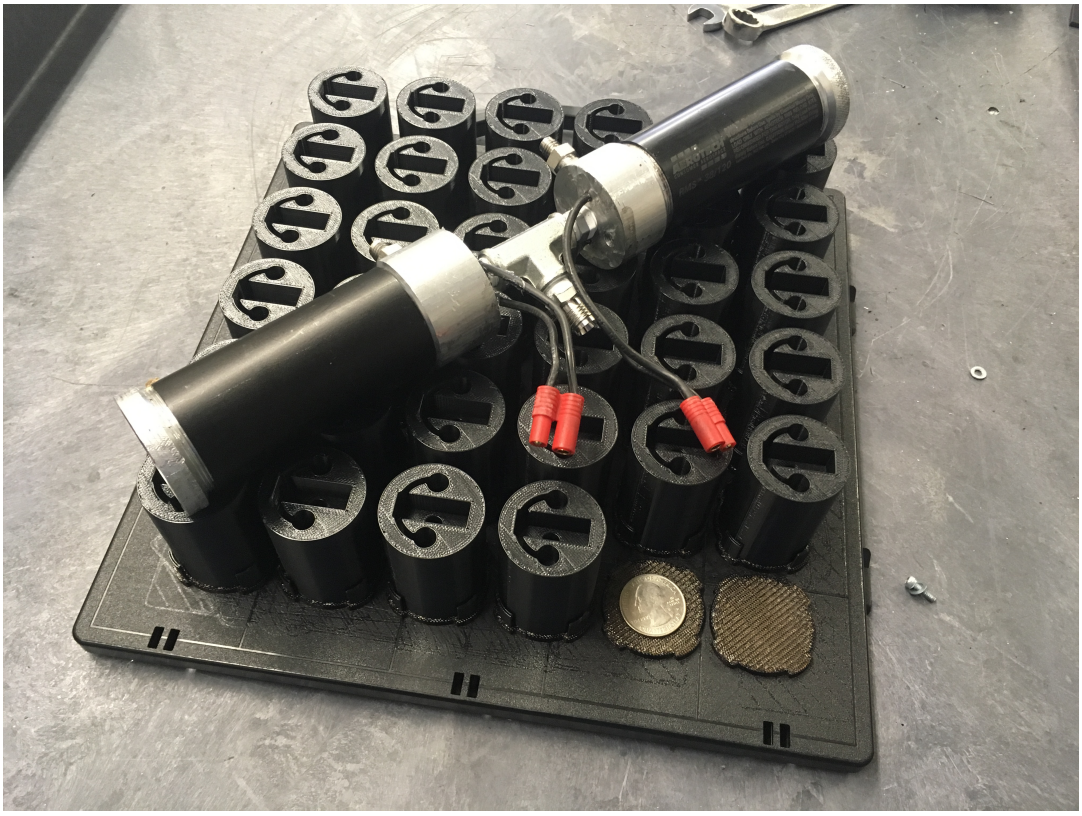

Fig. 3.3: Thruster Assembly on Tray of 36-3D Printed ABS Fuel Grains

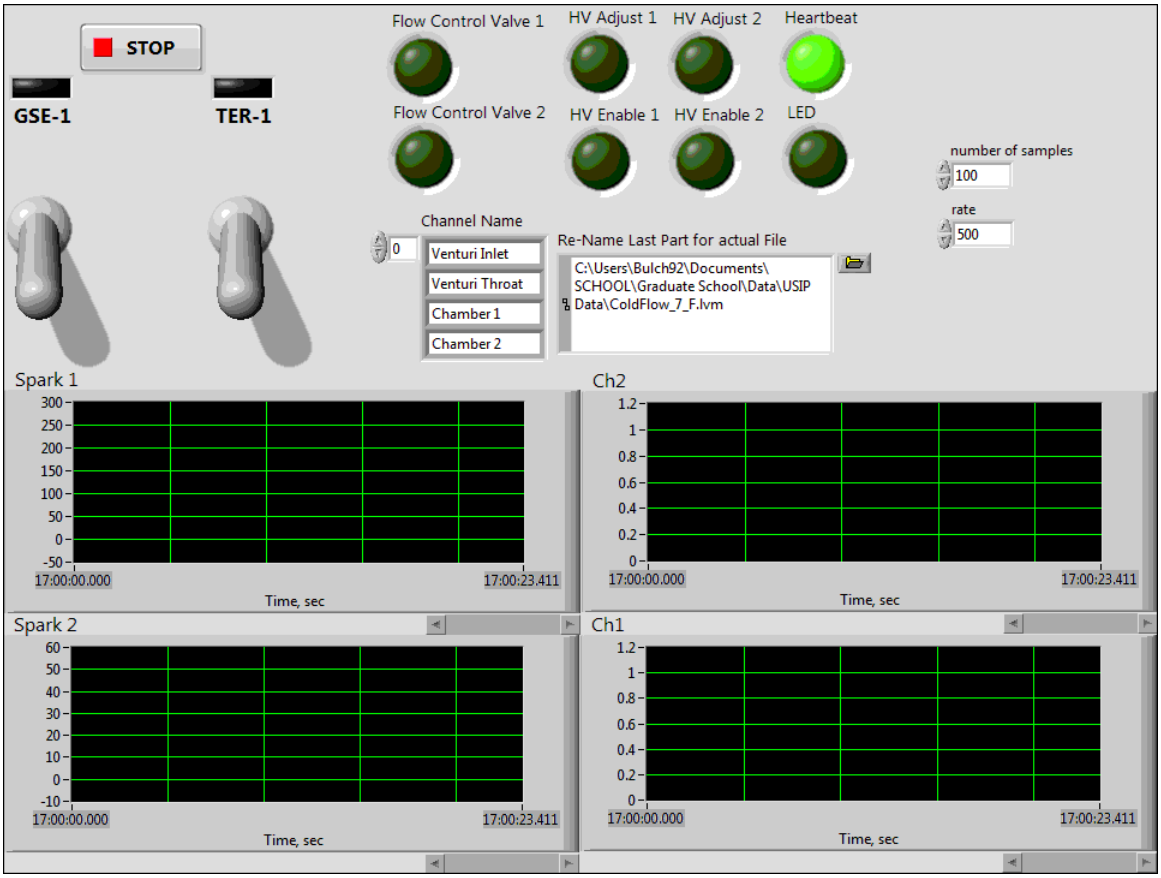

Fig. 3.4: Front Panel of Control Code used for USIP Assessment

TER-1 switch was flipped, which enabled the computer to run through pre-programmed ignition and burn sequences. The number and duration of thruster pulses grew from one to upwards of five throughout the testing campaign as the EAN40 thrusters grew more reliable. Each test helped to verify thruster performance and allowed further re-design to take place to better ensure a reliable and on-demand ABS/EAN40 thruster system. The results section will include data from ten EAN40 burns to highlight thruster performance and reliability.

3.3 Single Motor Test Layout

Aside from the dual motor USIP related testing, an array of single motor burns took place. In fact, it was on the single motor test stand that EAN40 was first tested. The single motor burns used one of the two motors attached to the USIP payload, ideally each of them being identical. The primary difference between these tests was that the single motor burns used varying O_2 concentrations at 55%, 75%, and pure GOX. The dual USIP motor configuration used only 40% O_2 concentration per NASA regulations and to provide evidence of reliable ignition and restarts for the sub-orbital flight. The USIP testing campaign proved sufficient to provide enough data to characterize the performance of EAN40. Figure 3.5 shows the setup for the single motor burns. The 38mm thruster is attached to the oxidizer flow path with 1/4" stainless steel line, which sits on aluminum T-slot railing. The T-slot railing sits on aluminum flexures allowing the test apparatus to flex backwards into the thrust-based load cell. Aft the thruster is a 24 Vdc solenoid valve, which controls the flow of oxidizer. At the tail end of the test cart lies the 25 lbf miniature load cell no larger in diameter than a quarter. Seen in the bottom left corner of Fig. 3.5 is the abort switch, which cuts power to the high voltage power supply and solenoid valve. This was a necessary safety feature in case of a control code glitch or Windows operating system error that could lead to an uncontrolled burn.

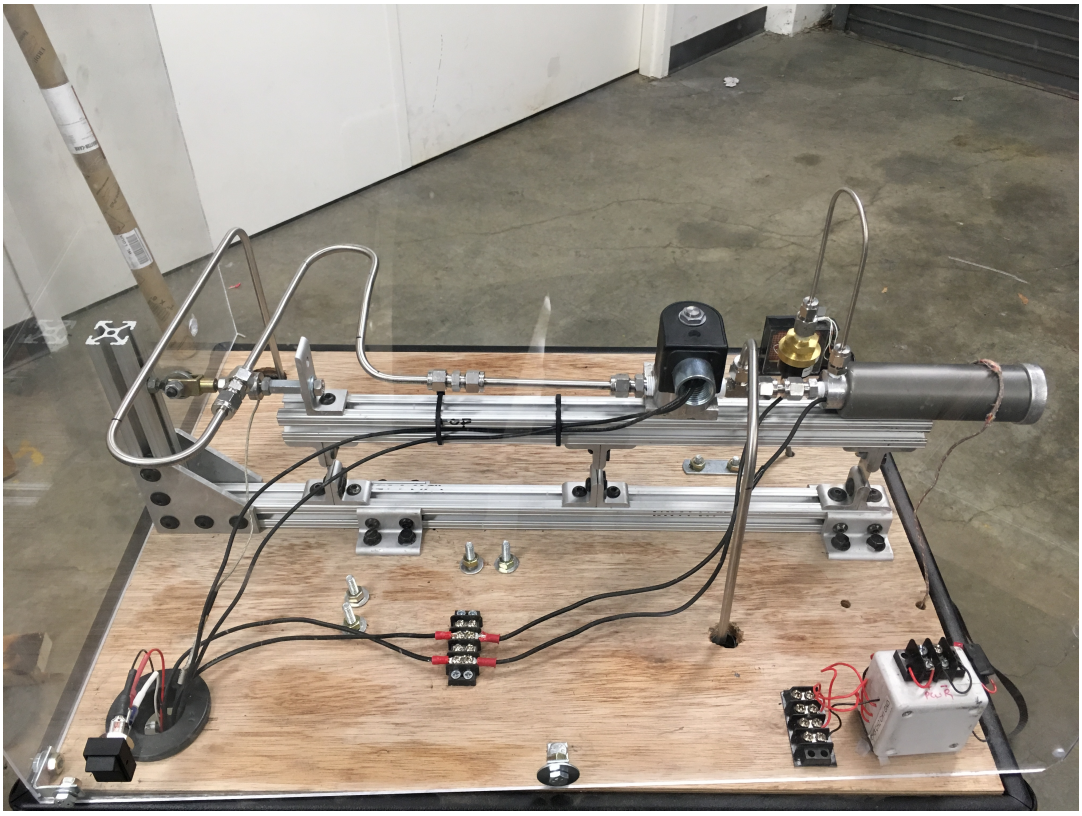

Fig. 3.5: Single Motor Burn Upper Test Deck

From the solenoid valve, the flow path winds back until feeding downwards to the middle deck of the test cart containing the mass flow venturi, pressure regulator, fill valve, and oxidizer tank shown in Fig. 3.6. The oxidizer tank was a Worthington high pressure compositive overwrap pressure vessel rated at 4500 psi operating pressure. The attached K-bottle valve was a simple scuba tank valve modified with CGA-540 PTFE O-rings to meet oxygen compatibility. A dial gage was installed to maintain situational awareness of the tank pressure upstream of the 3-way directional valve, which doubled as the fill valve.

During the Summer of 2017, tests were performed on this cart with the lower enclosed bay containing the control electronics. However, these were removed for another student's project and shipped to Huntsville, Alabama. In its place, another custom built instrumentation deck, shown in Figs. 3.7 and 3.8, was designed and built. This electronics box was made to be portable, with chest latches installed and the included power cable management

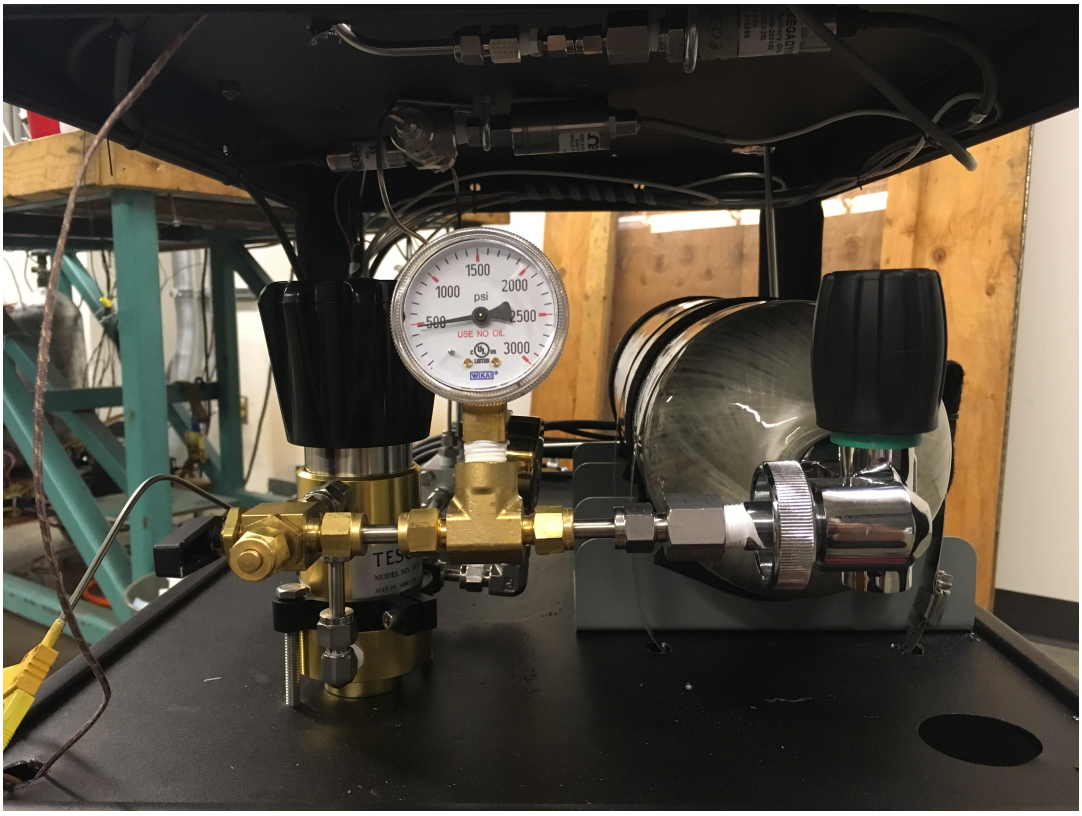

Fig. 3.6: Test Cart Middle Deck

Table 3.1: Instrumentation List of the Single Motor Tests

Transducer	
Chamber	Omega PX309-300GV
Venturi Inlet	Omega PX35D0-500GV
Venturi Throat	PX409-015DDUV
Load Cell	Omega LCCA 25 lbf
Thermocouple	Type K

system. The top side included 4-pin female amphenol connectors allowing quick connection of the pressure and load transducers and the high voltage-out terminal for the thruster ignition. Near the high voltage terminal is the power switch, which functions as a safety net for the ignition sequence. The two NI DAQ units shown are the USB 6002 (blue) and USB 6009 (white). The NI USB 6002 served to read and write data from several bridge transducers and as the controller for the high voltage signal via a single digital-out 3.2 volt signal. The NI USB 6009 was necessary to read an additional pressure measurement because the 6009 lacked sufficient analog input channels. The central portion shown in Fig 3.8 contains the power supplies mounted on a standard TS35 DIN rail, NI 9481 electromechanical relay, high voltage power supply, and the solenoid valve terminal in front. The NI 9481 served as the switching relay for single or dual solenoid valves depending on whether the tests were USIP related or single motor burns. Table 3.1 contains the list of transducers used to record data for the single motor burns.

In order to maintain test-to-test consistency, the single motor burns were fashioned after the dual motor tests because they were completed first. The dual motor burns were executed with a constant regulated pressure of approximately 450 psi, which led to an oxidizer mass flow rate less than 3 grams per second to each thruster. The chamber pressure during these tests typically exceeded 240 psi. To achieve some consistency with the single motor burns, the feed pressure was manipulated with a dummy fuel grain to produce similar chamber pressures for each degradation in O_2 concentration. For each concentration, five fuel grains

Fig. 3.7: Portable Instrumentation Deck - Top View

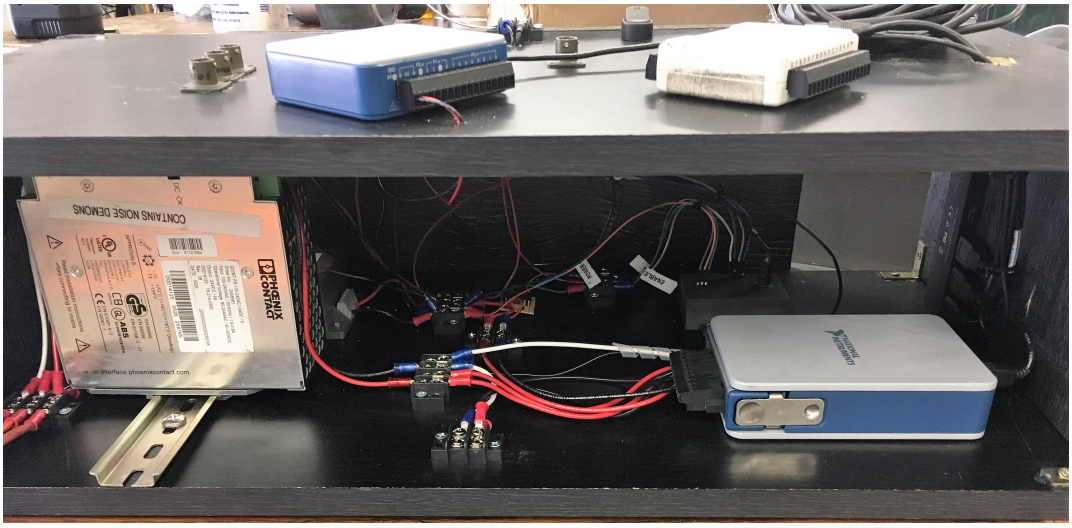

Fig. 3.8: Portable Instrumentation Deck - Front View

Table 3.2: Single Motor Burn Metric for Varied Concentration

Concentration [%]	Fuel Grains	Pulses	Pulse Duration [s]
100	5	3-4	2-3
75	5	4-5	3-5
55	5	4-5	3-5

were burned multiple times to achieve meaningful statistics. Table 3.2 summarizes the top level test layout for all the single motor tests. Results from the testing campaign of both the single and dual motor configurations will be presented in the results chapter of this thesis. Reliability, motor specific impulse, and regression rates will be presented. In addition, the sub-orbital flight test data will presented and thoroughly discussed in the next chapter.

CHAPTER 4

ANALYSIS, RESULTS, AND DISCUSSION

4.1 Analytical Methods

This section thoroughly details the calculations that were performed to evaluate the motor mass flow rates, specific impulses, O/F ratios and combustion efficiencies. The results are later used to compare the motor performance under various operating conditions. Section 4.1.1 describes the compressible flow equations that were used to calculate the oxidizer mass flow rate. Section 4.1.2 describes the method that was used to derive the total exit massflow, O/F ratio, and combustion efficiency. Section 4.1.3 details the fuel regression rate analysis approach using the fuel mass flow rate from section 4.1.2.

4.1.1 Compressible Flow Equations

The primary compressible flow equations presented in this section rely heavily on derivations performed in Anderson's Modern Compressible Fluid Flow [22]. The injector went through multiple re-designs throughout the USIP testing campaign. Simultaneous ignition of two small scale hybrid rockets that shared the same flow path had never been performed and proved to be challenging. The first challenge was the power management, and the second being the oxidizer mass flow rate. For the hybrid rockets to successfully ignite, build chamber pressure, and maintain a steady state burn the injector and nozzle throat had to experience choked flow. From heritage single motor burns using GOX, the injector was sized to ensure a maximum oxidizer flow rate of approximately 8 g/s [9] given the feed pressure remained under 400 psi. During the initial dual motor cold flow tests, the feed pressure was regulated to the same pressure to attain similar results. However, after multiple cold flow tests, the expected mass flow through each motor was less than predicted. This was because the two solenoid valves used on the USIP payload had a lower

flow coefficient than the valve used on the single motor test stand. The reason this change was made was due to the fact that the valves were meant for either vertical or horizontal orientation. The USIP payload would be nearly horizontal and in low gravity during its sub-orbital test so the decision was made to move to horizontal functioning solenoid valves. The flow coefficient was overlooked, and led to a maximum flow rate through the two valves at just under 7.5 g/s. Given the initial injector dimensions, the flow was choking upstream in one of the valves. Once this was discovered, the diameter of the injectors were sized accordingly. The equation used to size the injector is shown below in Eq. 4.1, which is the choking mass flow equation solved for the port diameter. Table 4.1 lists the key geometric parameters of the thruster, which remained consistent throughout this testing campaign.

$$D = \sqrt{\frac{4\dot{m}_{ox}}{P_0 \pi}} \left[\frac{\gamma}{R_g T} \left(\frac{2}{\gamma + 1} \right) \right]^{\frac{\gamma+1}{-4(\gamma-1)}} \tag{4.1}$$

In Eq. 4.1, the mass flow rate $\dot{m}$ was chosen to be a constant 3 g/s with plenty of margin regarding the solenoid valves maximum flow capacity. The pressure P_0 came from the upstream regulated feed pressure; however, regulator droop was not taken into account for this calculation. The gas constant R_g was changed depending on the O_2 concentration, though specific heat ratio γ was constant. The temperature T was measured using a thermocouple inline with the flow path upstream of the venturi.

Table 4.1: Motor Geometry

Parameter	**Injector**: Single Port, Diameter: 0.03 in.			
Fuel Grain	Diameter: 1.36 in.	Length: 1.96 in.	Weight: 43.0 - 43.5 g	Port Diameter: 0.20 in.
Motor Case	OD: 1.47 in.	Length: 3.25 in.	Wall Thickness: 1.7 mm	Material: Aluminum
Nozze	Throat Diameter: 0.076 in.	Exit Diameter: 0.154 in.	Expansion Ratio: 4.1	Nozzle Type: 5 deg. Conical

The last row in Table 4.1 explains the important nozzle characteristics. The nozzle was machined from a standard graphite rod with a simple conical design with an approximate exit angle of 5 degrees. The nozzle was designed with a 4:1 expansion ratio; however, due to errors associated with the lathing process, the expansion ratio was slightly larger at 4.1:1. At ambient conditions, the nozzle was intended to be slightly over expanded and was designed with the sub-orbital flight test in mind. Sufficient ground tests were performed with this nozzle to ensure the nozzle would be fully started in vacuum. Though, due to the large expected chamber pressures, all ground tests were performed with this identical nozzle. The nozzle throat and exit were measured periodically with miniature calipers having a resolution error of 0.0001 in., though no noticeable erosion was documented. Figure 4.1 shows a generic 2D drawing of a nozzle used as a baseline design throughout this testing campaign.

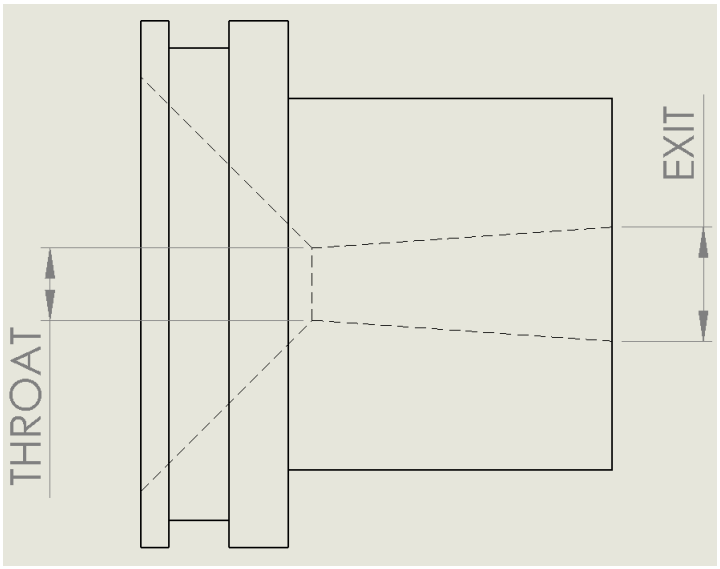

Fig. 4.1: Top Level 2D Nozzle

After the injector was determined to be functional, post-test analysis began by recording the sampling rate of the test data. Time-step biases were implemented in instances that captured fluid-mechanical response times and skewed the results of the oxidizer mass flow rate and the chamber pressure. To calculate the mass flow rate of oxidizer through

the system, the recorded inlet and throat pressures of the flow venturi were applied to the compressible unchoked mass flow equation, shown in Eq. 4.2.

$$\dot{m}_{ox} = C_d A_1 P_0 \sqrt{\frac{2\gamma}{R_g T(\gamma - 1)} \left[\frac{P_2}{P_1}^{\frac{2}{\gamma}} - \frac{P_2}{P_1}^{\frac{\gamma+1}{\gamma}} \right]} \tag{4.2}$$

The term P_0 is the stagnation pressure that was calculated using the compressible venturi mass flow equation. This was necessary to correct for the flow velocity within the venturi because the sensed inlet pressure was not the true stagnation pressure. The subscript "1" indicates the properties at the venturi inlet and the subscript "2" at the venturi throat. The discharge coefficient C_d was assumed to be 0.95, which represents a conservative figure based on ASME standards regarding the design of a venturi with a diameter ratio of $D1/D2 \approx 0.2$. The venturi inlet diameter was 0.2808", while the throat diameter was 0.125".

4.1.2 Determining the Fuel Mass Flow Rate and Mean O/F Ratio

The mass flow rate of fuel was checked independently by measuring the initial and final mass of the fuel grain and dividing by the steady state burn duration. For post-test analysis, a simple yet effective algorithm was implemented to determine a reliable flow rate of fuel. This process began by determining the combustion properties at each recorded point in the burn history using NASA's Chemical Equilibrium with Applications (CEA) code. CEA would output two dimensional thermodynamic tables at varying chamber pressures and O/F ratios, with the independent variables being the recorded chamber pressure, motor mean O/F ratio, and motor efficiency.

Figure 4.2 shows the block diagram that outlines the process used to determine the mass flow rate of fuel, motor mean O/F ratio, and motor efficiency. The process taken to determine motor performance follows this figure through the following description.

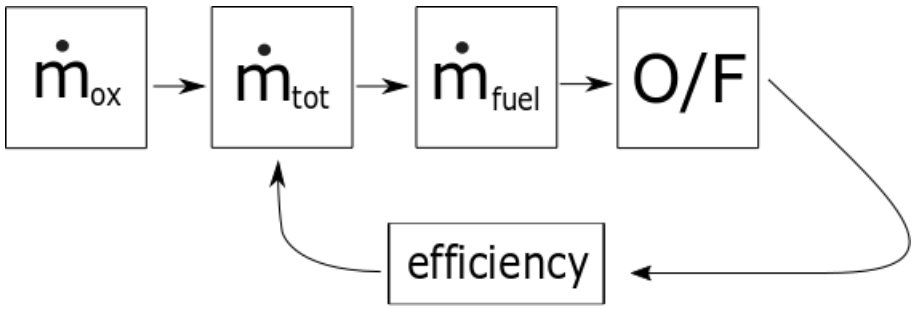

Fig. 4.2: Top Level Block Diagram of Analysis Sequence

The mass flow rate of oxidizer, $\dot{m}_{ox}$ was calculated using the methodology of section 4.1.1. Using CEA, the algorithm could be executed as outlined below. The total exit mass flow rate through the nozzle could be calculated using

$$\dot{m}_{total} = P_0 A_t \sqrt{\frac{\gamma}{R_g T_{0a}}} \sqrt{\left(\frac{2}{\gamma+1}\right)^{\frac{\gamma+1}{\gamma-1}}} \tag{4.3}$$

where A_t is the nozzle throat area and T_{0a} is the actual combustion flame temperature. The first cut mass flow rate of fuel could then be estimated:

$$\dot{m}_{fuel} = \dot{m}_{total} - \dot{m}_{ox} \tag{4.4}$$

The mean O/F ratio was determined by weighing the fuel grain post-burn and comparing that to the integrated exit fuel mass, M_{fuel}. The exit fuel mass was calculated by subtracting the oxidizer mass M_{ox} from the total exit mass M_{tot}. An example of the integrated exit mass components is shown below in Fig. 4.3 for a sample USIP burn. The mean O/F ratio was then calculated by dividing the measured consumed fuel by the known consumed oxidizer mass. This O/F ratio was then used as one of the independent look-up variables to the two dimensional thermodynamic CEA tables representing combustion properties.

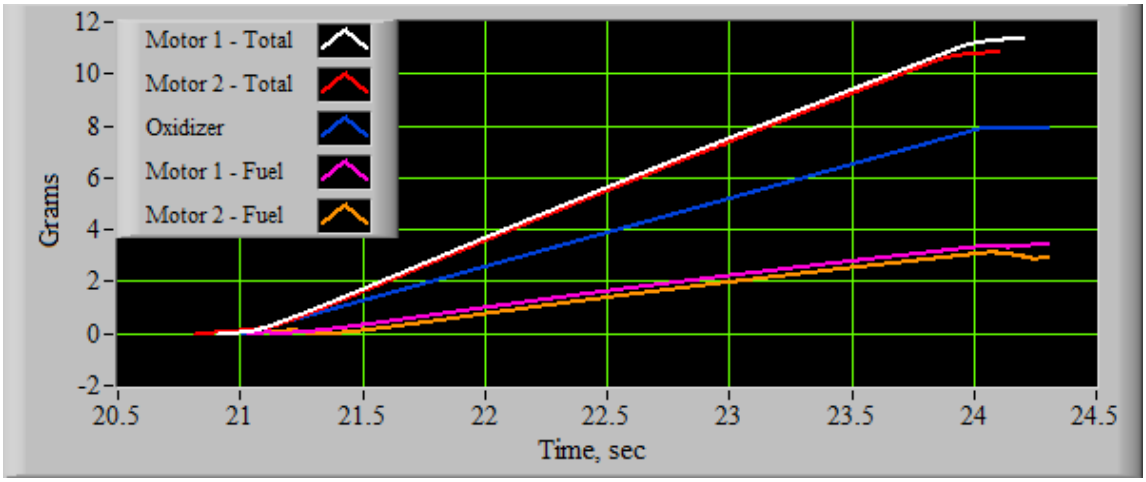

Fig. 4.3: Integrated Exit Mass

Once the mean O/F was determined, the motor burn efficiency was then adjusted to match the total exit mass flow rate from Eq. 4.3 with the summation of the known oxidizer mass flow rate and fuel mass flow rate using the following equation

$$T_{0a} = \eta^2 T_{0_{CEA}}; \tag{4.5}$$

where $T_{0_{CEA}}$ is the combustion temperature predicted by CEA. Adjusting the efficiency η adjusted the $\dot{m}_{total}$ output from Eq. 4.3, which led to the final step of evaluating the flow rates through the motor. Figure 4.4 shows the filtered total motor mass flow rates associated with the data from Fig. 4.3. By adjusting the motor burn efficiency, the total exit mass flow rate could be accurately determined.

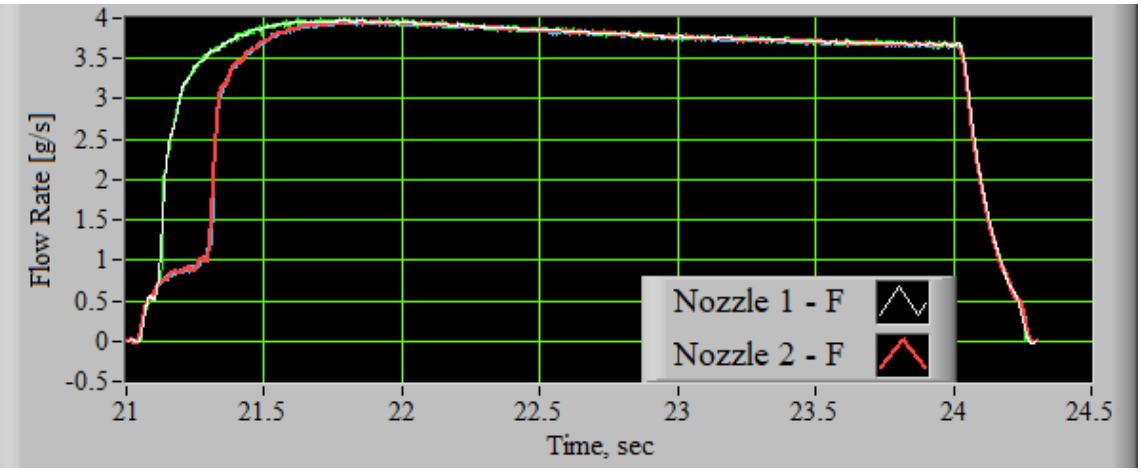

Fig. 4.4: Total Exit Mass Flow Rate

4.1.3 Fuel Regression

The fuel regression rate analysis was of particular interest due to the diminishing enthalpy of combustion of the chosen oxidizers, namely the concentrations highlighted in Table 3.2. Throughout many of the USU led research endeavors, pure oxygen has been used as the oxidizer. The regression rate as a function of oxidizer mass flux of a small scale 38mm motor, nearly identical in size to the thruster tested throughout this research, has been evaluated and is presented in the work performed by Merkley [16]. Peak fuel regression occurs at the beginning when the fuel port is at a minimum, then begins to slow as the fuel port opens. A 38mm ABS/GOX hybrid rocket exhibits a peak regression rate of approximately 0.26 cm/s, depending on the level of oxidizer mass flux. As will be shown in the results, the regression rate of the fuel does decrease with diminishing oxygen concentration, though not to the extent that may be assumed with an energy deficient oxidizer such as EAN40.

The regression rate derivation began by determining the volume of fuel at some time t.

$$V_{consumed} = \frac{M_{fuel}}{\rho_f} = \pi L(r(t)^2 - r_p^2) \tag{4.6}$$

Where ρ_f is the fuel density, $r(t)$ is the fuel port radius as a function of time, and r_p is

the initial port radius. Solving for $r(t)$ and taking the time derivative led to the regression rate equation shown below.

$$\dot{r} = \frac{\dot{m}_{fuel}}{2\sqrt{\rho\pi L}\sqrt{M_{fuel} + \rho\pi L r_p^2}} \tag{4.7}$$

The fuel regression rate was plotted against both time and oxidizer mass flux G_{ox} and will be presented in the results section. The mass flux is shown in the equation below.

$$G_{ox} = \dot{m}_{ox}(t)/A_p(t) \tag{4.8}$$

Where $A_p(t)$ is the area of the fuel port as a function of time.

4.2 Results

This section begins by describing preliminary results of the testing campaign performed using the baseline 38mm flight weight thruster. The flight weight thruster was tested at molar concentrations of oxygen ranging from 21% (air) to 100% (GOX). The following sections describe actual test results from a planned testing campaign to evaluate overall oxidizer performance. The ambient USIP dual motor tests and single motor tests were performed during the Spring of 2018 in the Propulsion Research Laboratory at USU. The test objectives included i) demonstration of successful ignition and restart capabilities using an industry recognized inert gas, ii) characterization of critical chamber pressure required for combustion seeding, and iii) characterization of motor rise time and ignition power variations. The motor rise time is defined as the time elapsed from flow valve initiation to 85% of the maximum steady state chamber pressure. In addition to these goals, thrust and specific impulse values are presented with the tested 4.1:1 expansion ratio nozzle. The discussion section addresses the model predictions, shortfalls, and the motor regression study across all evaluated oxidizers.

4.2.1 Preliminary Test Results

In this initial test series, to establish a baseline, the motor was first burned using pure GOX at various chamber pressures to assess the onset combustion pressure. The GOX was then replaced with compressed air with increasing levels of enrichment from 21% to EAN32, EAN36, and 40%. For this testing campaign, upstream feed pressure was increased in increments of approximately 25 psia from 25 to 150 psia. The successful ignition and sustained combustion of ABS fuel with compressed air relies on two features: 1) oxidizer flow rate large enough to choke the nozzle throat to ensure a rapid increase in chamber pressure and 2) oxidizer feed pressure approximately two times greater than any expected operating chamber pressure to ensure a choked injector.

From this test series, it was universally discovered that reliable arc ignition could be achieved once the partial pressure of O_2 in the thrust chamber exceeded approximately 2 atmospheres. These tests characterized the previously observed chamber pressure of approximately 2 atmospheres required to seed combustion with pure GOX.

Figure 4.5 shows a typical EAN40 chamber pressure curve from the oxidizer evaluation test series. The sharp rise in chamber pressure occurs between 70 and 80 psia, indicating an approximate partial pressure of oxygen of two atmospheres. These results are shown for 25 ignition tests using standard air, EAN32, EAN36, EAN40, and GOX, with chamber pressures varying from 25 to 150 psia in Figure 4.6.

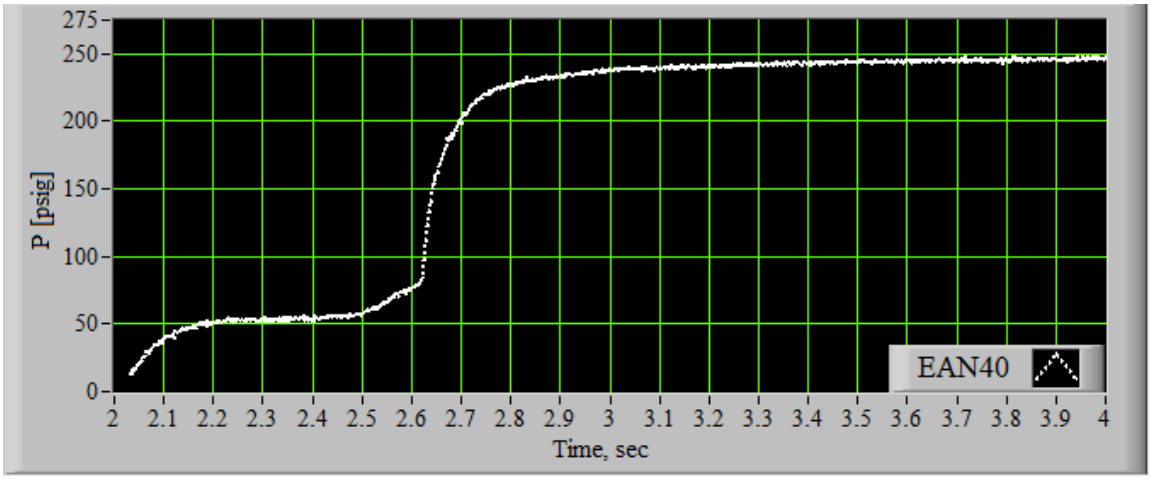

Fig. 4.5: Chamber Pressure Curve of an EAN40 Test

On this figure, the steady chamber pressure is plotted on the x-axis, and the molar concentration of O_2 is plotted on the y-axis. The solid black curve represents a curve fit, which indicates the required 2 atmospheres of O_2 partial pressure. The black symbols represent successful ignitions, and the red symbols represent tests where the motor failed to ignite.

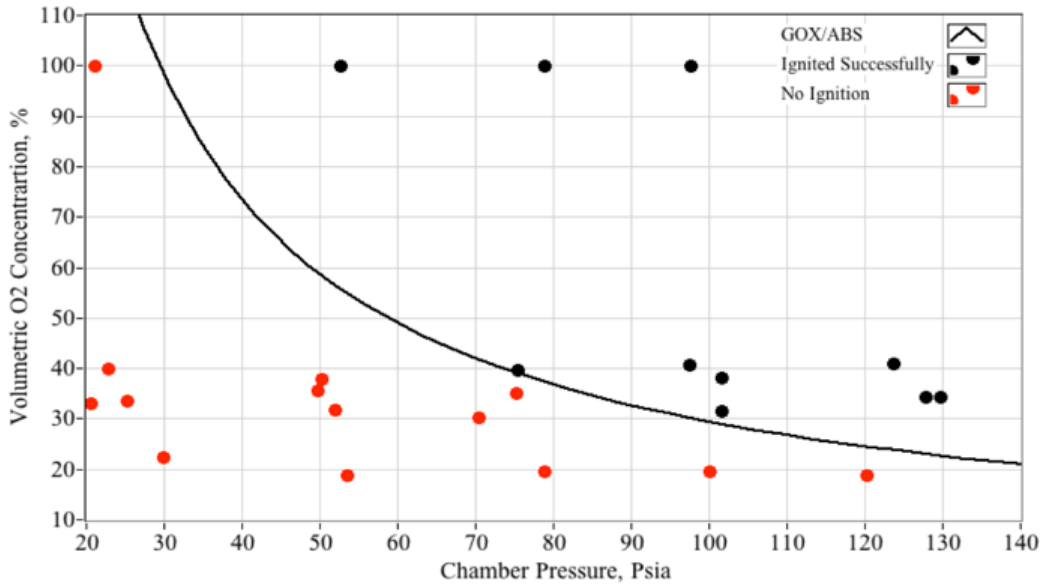

Fig. 4.6: Minimum Molecular Oxygen O_2 Concentrations Required for Successful Ignition

4.2.2 Ambient Condition Test Results

The EAN40 USIP dual motor burns were executed with a constant regulated feed pressure of approximately 450 psig, which led to an oxidizer mass flow rate less than 3 grams per second to each thruster. The chamber pressure during these tests typically exceeded 240 psia, indicated in Figure 4.5. To maintain test-to-test consistency, the single motor burns were fashioned after the USIP dual motor tests. The feed pressure was adjusted with a dummy fuel grain to produce similar chamber pressures for each degradation in O_2 concentration. For each concentration, five fuel grains were burned multiple times to produce meaningful statistics. However, the USIP tests doubled the consumed fuel grains for the EAN40 testing due to the self-nulling configuration, yielding 10 samples of burn data. Table 4.1 summarizes the top-level test logic for the flight weight thrusters.

Table 4.2: Burn Summary at Varied O_2 Concentrations

Oxidizer	**Fuel Grains**	**Burns**	**Burn Duration** [s]
EAN40	10	4-5	3-4
55%	5	4-5	3
75%	5	4-5	3
100% (GOX)	5	3-4	2-3

1.) *EAN40 Test Summary*

The USIP dual motor tests comprised of 10 fuel grains all burned using EAN40 and with identical regulated feed pressures. The mean thrust level was approximately 5.07 N with a burn-to-burn standard-deviation of 0.50 N. At the 95% confidence level, the estimated error for the mean thrust level was 0.36 N. The mean Isp was approximately 136.6 s, with a burn-to-burn standard-deviation of 10.4 seconds. At the 95% confidence level, the estimated error for the mean Isp was 7.4s. The mean ignition power was 2.42 W 2.19 W with an

estimated error of 1.56 W. Lastly, the motor rise time had a mean value of 362 ms 73 ms with an estimated error of 52 ms.

The quoted average I_{sp} is lower than expected; however, the motor rise time affects the overall performance of the motor. In comparison to a heritage USU green thruster [9], the I_{sp} data presented here are from tests using less than half the mass flow rate of oxidizer. This was part of the overarching goal of decreasing the thrust levels, while maintaining some level of consistency and performance. During a standard 3 second burn, the motors tested with EAN40 regularly experienced greater than 12% of the total burn at pressures and temperatures comparable to a cold gas system. With such a low pressure plaguing the startup transient, the average I_{sp} is greatly reduced on a burn-to-burn basis. However, the peak I_{sp} on a burn-to-burn basis using EAN40 consistently achieved values upwards of 165 seconds, similar to the initial preliminary tests. Figure 4.7 shows the specific impulse curve from an EAN40 motor test that exhibited a rise time lower than average and shows the peak I_{sp} greater than 160 seconds.

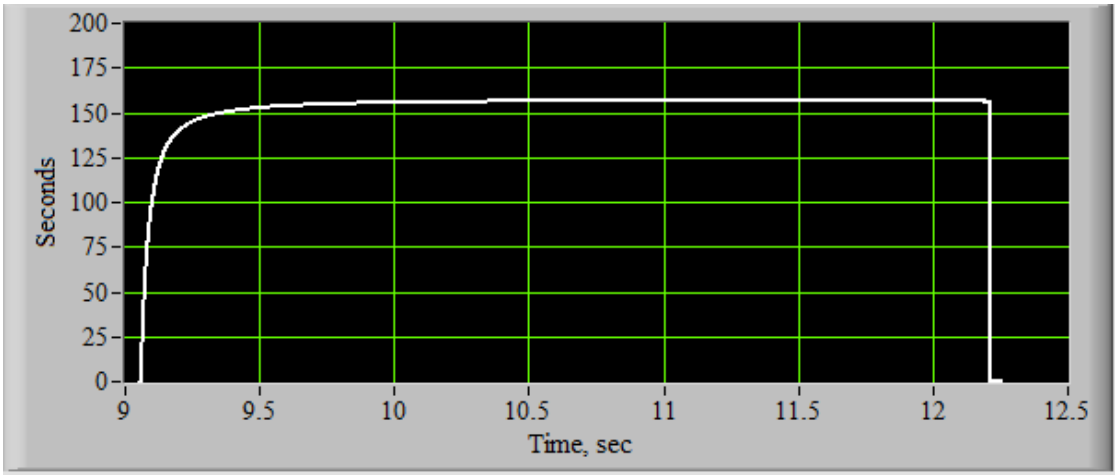

Fig. 4.7: Specific Impulse Curve for an EAN40 Test

2.) *55% Test Summary*

The testing of EAN55 comprised of 5 fuel grains all burned with identical regulated feed pressures. The mean thrust level was approximately 5.13 N with a burn-to-burn standard-

deviation of 1.97 N. At the 95% confidence level, the estimated error for the mean thrust level was 0.25 N. The large standard deviation in the thrust was a result of several tests with large startup up transient. The mean I_{sp} was approximately 140.7 s, with a burn-to-burn standard-deviation of 9.7 seconds. At the 95% confidence level, the estimated error for the mean Isp was 12.1s. The mean ignition power was 2.46 W 0.87 W with an estimated error of 1.08 W. Lastly, the motor rise time had a mean value of 430 ms 98 ms with an estimated error of 122 ms.

The EAN55 evaluation testing was surprisingly difficult in the sense that obtaining a moderately consistent rise time, and hence I_{sp} and thrust was near impossible. The fuel grains, ignition sequence, and test conditions remained identical throughout this testing campaign so a reason as to why these irregularities occurred is unknown. Regardless of the acquired test data, the data was analyzed all the same and input into the statistics model. The statistics, as compared to EAN40 are not as favorable; however, EAN40 had double the number of fuel grains because of the USIP related testing, which led to a smaller student-t table constant and a greater degree of freedom.

3.) *75% Test Summary*

The testing of EAN75 comprised of 5 fuel grains all burned with identical regulated feed pressures to achieve the sought after 250 psia chamber pressure. The mean thrust level was approximately 5.09 N with a burn-to-burn standard-deviation of 0.51 N. At the 95% confidence level, the estimated error for the mean thrust level was 0.64 N. The mean I_{sp} was approximately 160.2 s, with a burn-to-burn standard-deviation of 17.9 seconds. At the 95% confidence level, the estimated error for the mean I_{sp} was 22.3s. The mean ignition power was 1.50 W 0.37 W with an estimated error of 0.46 W. The motor rise time had a mean value of 208 ms 60 ms with an estimated error of 74 ms.

The EAN75 evaluation testing was similar in all aspects, besides performance, to that of USUs heritage GOX burns. The rise time was faster than the lower energy EAN55 and the baseline EAN40. The power requirement was on average 1 W less than the lower energy burns as well, even though the same high voltage spark logic was implemented across all

tests. The large I_{sp} standard deviation was a result of several tests having an increased rise time. This affects the overall motor performance including thrust and mass flow rates, which are directly related to the motor I_{sp}.

4.) *GOX Test Summary*

The testing of GOX comprised of the typical array of 5 fuel grains all burned with identical regulated feed pressures to achieve the 250 psia chamber pressure. The mean thrust level was approximately 5.46 N with a burn-to-burn standard-deviation of 0.23 N. At the 95% confidence level, the estimated error for the mean thrust level was 0.28 N. The mean I_{sp} was approximately 175.5 s, with a burn-to-burn standard-deviation of 5.7 seconds. At the 95% confidence level, the estimated error for the mean I_{sp} was 7.1s. The mean ignition power was 1.94 W 0.24 W with an estimated error of 0.29 W. The motor rise time had a mean value of 230 ms 104 ms with an estimated error of 129 ms.

The GOX evaluation testing operated in a near identical fashion to USU heritage GOX burns. The primary differing factor with these tests was the very small mass flow rate of oxidizer. Previous year evaluations tested the ABS/GOX motor with oxidizer flow rates between 6 and 9 grams per second with injector and nozzle throat diameters of 0.05 and 0.125, respectively. With the current geometry, and the given regulated feed pressure to achieve chamber pressures around 250 psia, the oxidizer mass flow rate was approximately 2.5 grams per second. At these low mass flow levels, greater inconsistencies in the motor rise occurred than previous tests that had sufficiently large oxidizer flows to rapidly increase chamber pressure. Previous evaluations with larger injector and nozzle throat geometry produced a mean I_{sp} of 200 seconds. However, due to the small scale of these motors in combination with nearly identical mass flow rate of fuel seen during previous experiments, the mean I_{sp} of the pure GOX decreased, as expected.

Table 3 summarizes the ground tests using the oxidizers EAN40, 55%, 75%, and pure GOX. Many of the key performance characteristics of this green thruster are listed including the mean thrust, specific impulse, ignition power, rise time, and corresponding sample standard deviation along with each testing campaigns 95% confidence intervals, represented

by σ. All tests used a 4.1:1 expansion ratio nozzle and were evaluated in Logan, UT with an approximate background pressure of 86 kPa. The tested expansion ratio nozzle was not optimized for the background pressure, with an ideal expansion ratio being 3.4:1. However, optimizing the nozzle was not a key factor in determining ambient motor test performance. The motor ignition power varied far and wide across all oxygen concentrations. However, there is a clear distinction between the two lower concentrations, EAN40 and EAN55, with the two higher concentrations. Somewhere between 55% and 75% oxygen, the high voltage spark path across the fuel grain drops in voltage. This was an unexpected result and at this time remains unexplained. Though, it should be restated that all testing used the same PPU and applied the same spark timing to each ignition sequence. In a similar manner, the motor rise sees the exact same trend as the ignition power. With lower concentrations of oxygen, it takes longer for the partial pressure of oxygen to reach two atmospheres. With similar flow rates across all tested oxidizers, as the concentration increased, the average rise time decreased.

Table 4.3: Summary of Ground Test Results

Case	**Nozzle Area Ratio**	**Ambient (Feed) Pressure [kPa]**	**Thrust [N]**	**Isp [s]**	**Ignition Power [W]**	**Rise Time [ms]**
EAN40	4.1:1	86 (3310)	$\mu = 5.07 \pm 0.50$ $\sigma = \pm 0.36$	$\mu = 136.6 \pm 10.4$ $\sigma = \pm 7.4$	$\mu = 2.42 \pm 2.19$ $\sigma = \pm 1.56$	$\mu = 362 \pm 73$ $\sigma = \pm 52$
55%	4.1:1	86 (2690)	$\mu = 5.13 \pm 1.97$ $\sigma = \pm 0.25$	$\mu = 140.7 \pm 9.7$ $\sigma = \pm 12.1$	$\mu = 2.46 \pm 0.87$ $\sigma = \pm 1.08$	$\mu = 430 \pm 98$ $\sigma = \pm 122$
75%	4.1:1	86 (2380)	$\mu = 5.09 \pm 0.51$ $\sigma = \pm 0.64$	$\mu = 160.2 \pm 17.9$ $\sigma = \pm 22.3$	$\mu = 1.50 \pm 0.37$ $\sigma = \pm 0.46$	$\mu = 208 \pm 60$ $\sigma = \pm 74$
GOX	4.1:1	86 (2230)	$\mu = 5.46 \pm 0.23$ $\sigma = \pm 0.28$	$\mu = 175.5 \pm 5.7$ $\sigma = \pm 7.1$	$\mu = 1.94 \pm 0.24$ $\sigma = \pm 0.29$	$\mu = 230 \pm 104$ $\sigma = \pm 129$

4.2.3 USIP Sub-Orbital Flight Test Results

On March 25th, 2018, at 6:51:30 EDT, after multiple launch delays due to bad weather caused by an unseasonably late "Nor-Easter" off of the east coasts, the two-stage Terrier-Improved Malemute sounding rocket named "Viera" in honor of retired flight director Jack Viera launched from Wallops flight facility. The launch was entirely successful with and achieved apogee of 172 km. The payload, shown in Fig. 3.1, achieved more than 6 minutes above the Von-Karman line. The payload section was successfully recovered by WFF flight

support.

During the mission the USU ABS/EAN40 "green" hybrid thruster was successfully fired 5 times in a hard vacuum environment above the Von-Karman line. Low-resolution telemetry data was successfully downlinked and delivered to USU for analysis. This data was demodulated, time-tagged, and converted to engineering units. A preliminary analysis of the motor performance was performed soon after launch before the ocean-soaked flight computer was successfully re-booted. Figure 4.8 presents a panel of the downlinked telemetry.

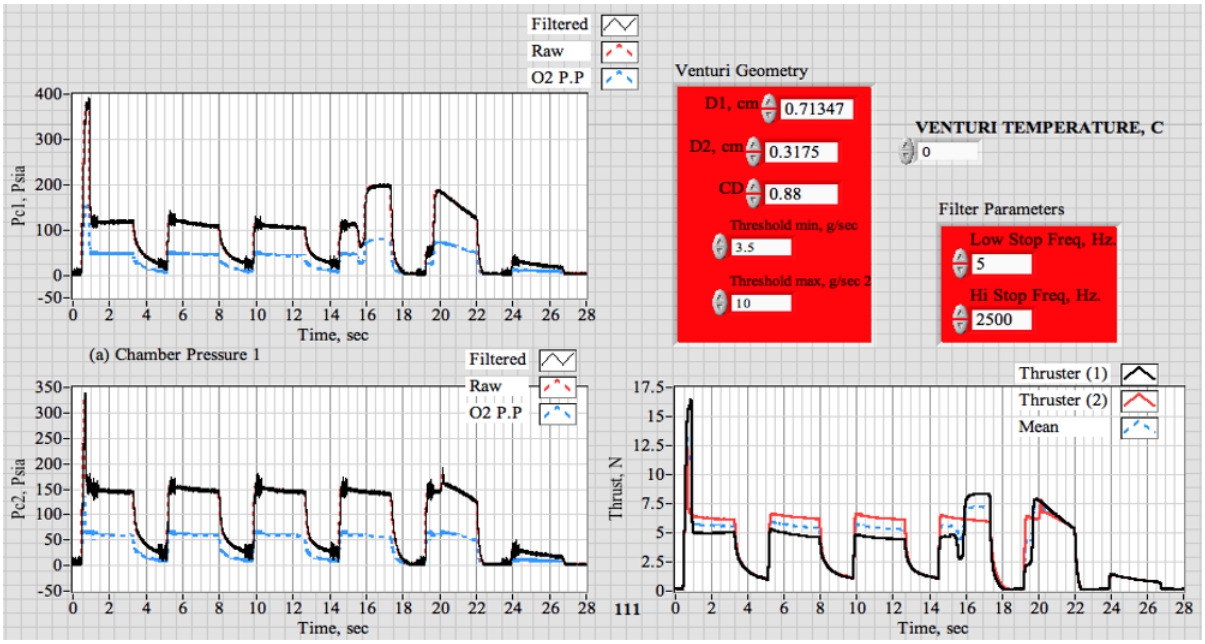

Fig. 4.8: Low Resolution Downlink Data from USIP Launch

Besides the large initial spike in chamber pressure, the motors appear to be operating similarly to ground tests. The absence of background pressure produced faster rise times, as was expected based on previous soft-vacuum tests. However, the first three pulses operate at chamber pressures approximately 100 psi below expected values. It is not until the fourth pulse that motor 1 reached 200 psia, though all ground tests were burning at 250 psia. It was discovered that the regulator had been unintentionally adjusted throughout integration, decreasing the oxidizer feed pressure to the motors. This could have happened at any point

after arriving at Wallops on Friday, March 16th. The payloads were inspected by NASA personnel, handled by various engineers, and underwent several integration sequence tests leaving room for accidental manipulation. This change in feed pressure negatively impacted the overall performance of the ABS/EAN40 hybrid thrusters, though it did not affect the motor ignition sequence.

After recovering the actual flight data from the flight computer, a higher fidelity investigation of the data led to a better understanding of what occurred. A pulse-to-pulse I_{sp} of the first three burns averaged between 115 and 155 seconds for motor 1 and motor 2, respectively, with pulse 3 being shown in Fig. 4.9. The data curves in the beginning of Fig. 4.9 appear erratic due to the tail-off pressure of the previous burn, which was a result of the the small nozzle throat area. Though, overall motor evaluation was not affected by this motor feature. These numbers are proof that ABS fuel was being vaporized, though not to the degree that was originally planned and at a high oxidizer-to-fuel ratio. These high specific impulse numbers, relatively speaking, could not have been attained if only cold gas was being injected into the thruster port. When motor 1 achieved full ignition for 1.5 seconds during the fourth pulse, peak I_{sp} reached 200 seconds. Had the nozzle been manufactured from a refractory metal, easily allowing an expansion ratio of 50:1 - a value typically low for hydrazine monopropellant thrusters - peak I_{sp} would have reached 220 seconds.

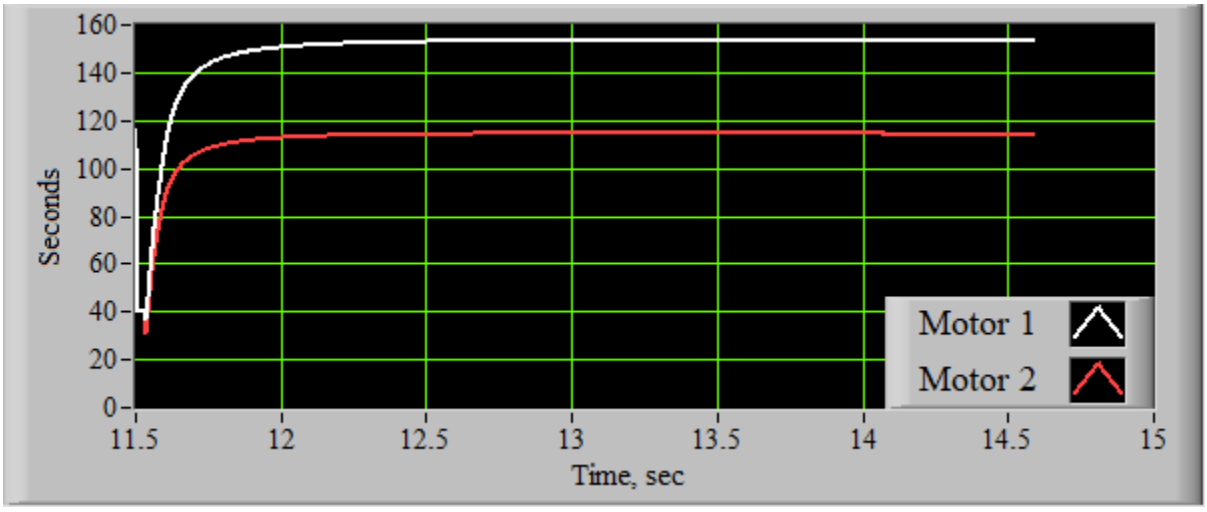

Fig. 4.9: Specific Impulse of High O/F Low Pressure Flight Test

Based on these results, it is concluded that the first three burns did not reach the expected peak operating chamber pressure. The expected thrust level dropped as a result to approximately 5 N, even though each motor was receiving an approximate 2.5 grams per second of EAN40 oxidizer, slightly less than during the multiple ground tests. From the observed 120+ psi in motor 1, and 150+ psi in motor 2 along with the observed pressure spike in motor 1 during the fourth burn, it was determined that a low energy, high O/F smoldering type burn was achieved. The large indicated chamber pressure across all 3-second pulses indicate that ABS fuel was being vaporized, because all preliminary cold flow ground tests never exceeded 60 psia. This also indicates that the ignition sequence was fully functional and the spark path of each fuel grain was operational across all 5 motor ignitions, in addition to the 6th pulse that was planned to blow down the tank pressure to near ambient.

4.2.4 Post Launch Ground Simulation - Freeze Tests

The Terrier Malemute was mated to the launch rails on Wednesday, March 21st. Originally, the plan was for a 24 hour wait period before launch on Thursday, March 22nd. However, adverse weather conditions delayed the actual launch until Sunday, March 25.

The integrated vehicle remained on the launch rail for 4+ days while waiting for clear weather. The test team has concluded that the highly-porous 3-D printed ABS fuel grains had partial water condensation throughout due to the 4+ days sitting on the rail and exposed to the violent weather of a late season nor-easter storm. The day of launch dawned cold and clear with temperatures in the low 20s F. It is very likely that any entrapped moisture in the fuel grains was frozen solid.

A series of ground-experiments were completed that indicate this assumption to be true. These follow-on experiments involved briefly dipping the grains into water and then placing them in a freezer. Once the fuel grains were frozen, they were inserted into the motor case with attached injector and nozzle caps and placed again into the freezer. These tests mimicked the USIP test with identical 3-second pulse series with EAN40 as the oxidizer, and showed very similar results to those obtained in Fig. 4.8. The primary difference was the fact that it only required two pulses to clear away the entrapped water that was halting successful ignition. Figure 4.10 shows one of the post-launch freeze burns, which is representative of what was observed for three post-launch EAN40 freeze tests. Disregarding the surge in chamber pressure at the tail end of the second pulse, it can be determined that the presence of frozen water within the fuel grains impacted the motors ability to seed combustion. Oddly enough, the chamber pressure remained around 60 psi during the first pulse, providing further evidence of a low energy smoldering type burn exhibited by the USIP flight data. Successful ignition and steady state burn was consistently achieved on the frozen fuel grains during the third burn, as opposed to the fourth burn on the USIP sub-orbital flight test.

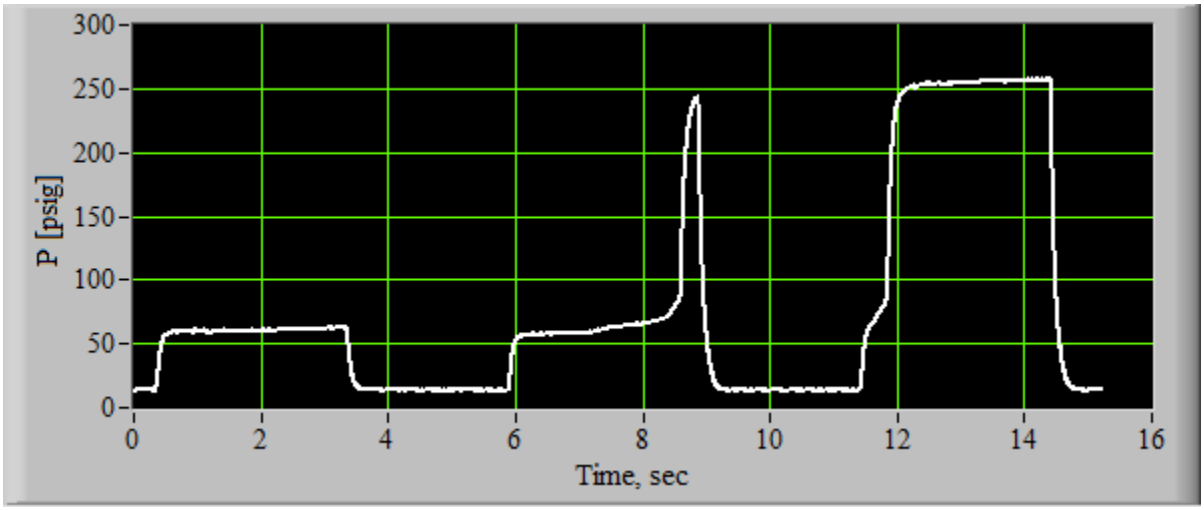

Fig. 4.10: Chamber Pressure Curves of Post Launch Frozen EAN40 Test

As a sanity check to these post-launch frozen tests, one of the fuel grains was tested with GOX. This was done to see if a change in oxidizer would have any affect on the frozen grains startup transient. Figure 4.11 shows the chamber pressure curves on a water-soaked frozen fuel grain with GOX. Clearly, any entrapped water was instantly vaporized due to the high enthalpy of combustion of ABS and GOX. In fact, it should be noted that the enthalpy of combustion of ABS and EAN40 at the operating O/F ratios exceed the enthalpy of vaporization of ABS by approximately 25%. This can be seen by the plot shown in Fig. 4.11. This figure was made using CEA and plotting the product of specific heat and combustion temperature assuming equilibrium composition during expansion from the infinite area combustor. Figure 4.11 shows how the enthalpy of combustion of the ABS/EAN40 mixture is only slightly larger than the 3.1 MJ/kg required to vaporize solid ABS fuel at the experimentally observed average O/F ratio of 2 [16]. Had the flight test used GOX, it would be expected to see results nearly identical to those in Fig. 4.12.

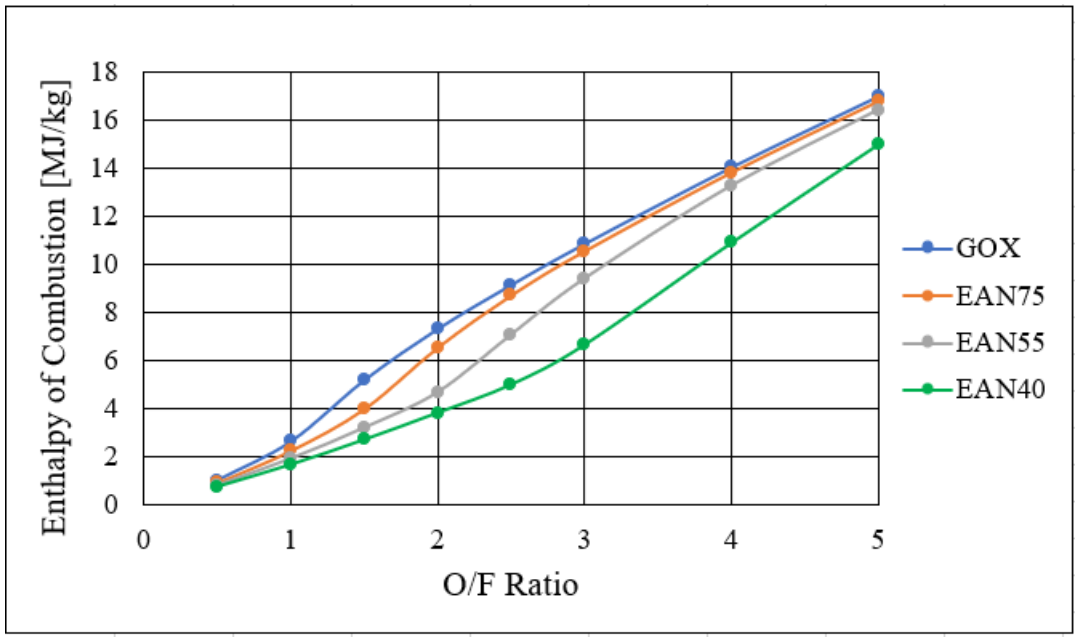

Fig. 4.11: Enthalpy of Combustion Plotted at Varying O/F Ratios

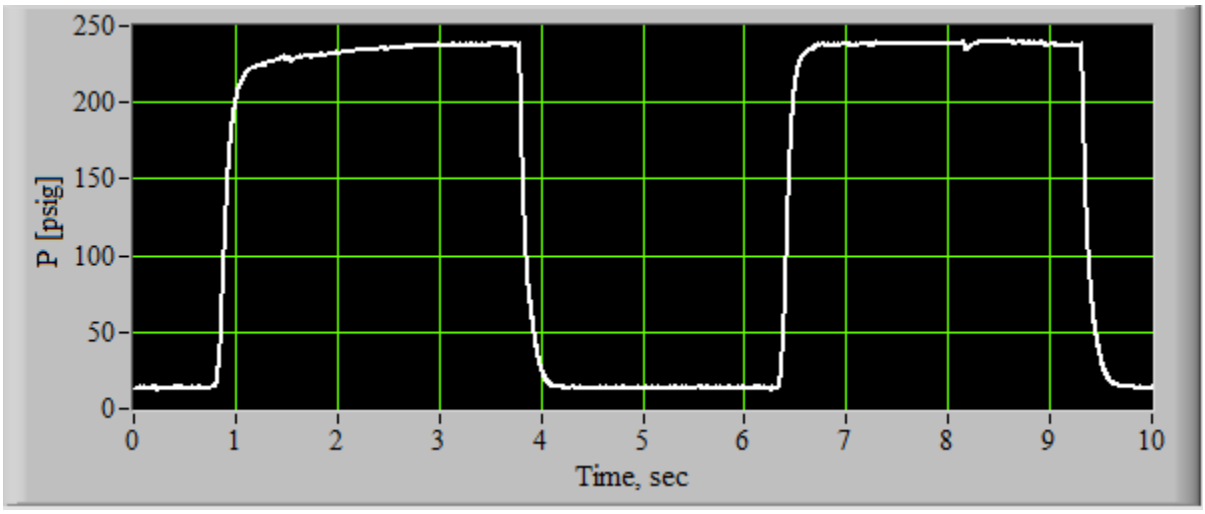

Fig. 4.12: Chamber Pressure Curves of Post Launch Frozen GOX Test

During the sub-orbital flight, it took 3+ burns in order for the ignition pyrolysis to clear away the entrapped water and allow for full combustion. Full combustion was finally achieved at approximately 16 seconds into the experiment. This event is noted by the sharp

rise in chamber pressure and thrust time history traces for the starboard thruster. At this point the thruster achieved a 6 N thrust level and 200 second specific impulse predicted by the flight test analysis. Obviously, sitting on the launch rail for 5+ days during a violent late winter mid-Atlantic storm represents less than ideal launch conditions. The fact that the non-ruggedized system worked at all is a testament to the robustness of the overall design.

4.3 Discussion

Up to this point, the content of this thesis has spoken primarily on background, test setup, and lab test results. The analytical model used to predict specific motor performance, described in section 2.2, produced skewed results and did not compare well with experimental outcome. The content from [16] investigated radiation heat transfer effects in hybrid rocket ballistics of small scale motors, and determined that with motor length-to-diameter (L/D) ratios approaching 2, modeling begins to break down. The motor presented throughout this paper had a fuel grain L/D ratio of approximately 1.40. However, an effort was made to manipulate parameters such as the burn exponent n, the skin friction coefficient C_f, and heat transfer mechanisms such as emmisivity ϵ and absorbtivity α to produce results similar to experimental outcomes.

The burn exponent n varies between 0 and 1, with larger scale motors exhibiting exponents greater than 0.5, which indicates a positive O/F shift throughout the burn. This is a commonly observed trait in motors with an L/D greater than approximately 3, and is highlighted by work completed by Marshall [23]. When the burn exponent equals 0.5, the O/F ratio remains constant during the burn, a trait common in paraffin based fuels. However, when the L/D ratio is approximately 2 or below, the burn exponent is less than 0.5, indicating a progressively richer exhaust plume as the fuel port opens. This was observed throughout every test performed on these motors. Therefore, prescribing a burn exponent of 0.4 in the analytical model seemed appropriate.

However, it was discovered throughout modeling that with decreasing the burn exponent, the predicted starting O/F ratio would increase even though the general lean-to-rich

trend remained consistent. The heat transfer terms were manipulated as well; however with emissivity values above 0.5, the model would output highly erratic predictions, as shown in the O/F ratio curve of Fig. 4.13.

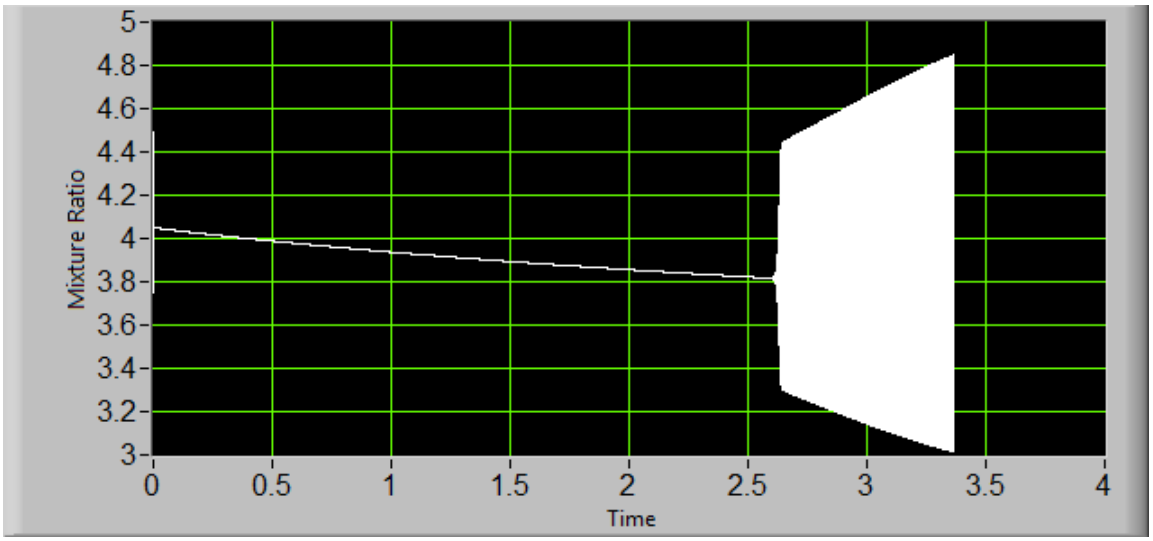

Fig. 4.13: Model Prediction of O/F Ratio with Emissivity of 0.6

A relationship was discovered between the skin friction coefficient and the burn exponent, that being an increase in C_f decreased the burn O/F ratio, nulling the leaner-burn effects of decreasing the burn exponent. This was taken advantage of until the model could be successfully run with burn exponents below 0.5. Though the model was successfully run at burn exponents less than 0.5, the chamber pressure was under predicted, the thrust was over predicted, and as a result the specific impulse was over predicted. These factors, when combined, under predicted the fuel regression rate, which was observed by the uncharacteristically high O/F ratios shown in Fig. 4.13, with experimentally observed values remaining below 2.6. The fuel regression rate prediction was off by more than 40% when compared to experimental outcomes. These model results agree wholeheartedly with the radiation heat transfer investigation of hybrid rocket fuel regression mentioned above. At the time of this thesis, predictions of the fuel regression rate in small scale, low mass flux hybrid rockets remain inaccurate.

From observing the exhaust plume during tests, it was determined that the burn exponent had to be less than 0.5. To evaluate the true burn exponent exhibited by the varying oxidizer combinations, analysis methods of section 4.1.3 were implemented. Shown in Fig. 4.14 is the fuel regression rate plotted against the oxidizer mass flux for both GOX and the oxidizer containing an oxygen concentration of 75%. The data points were all collected at identical points throughout the tests. During each burn, regardless of burn duration, the instantaneous regression rate and oxidizer mass flux was recorded. Fitting the data points with an exponential curve fit in the form of $\dot{r} = aG_{ox}^{n}$ led to the determination of the scale factor and burn exponent.

Previous investigations have determined that these factors change as the scale of the motor increases or decreases. For the 38mm motor described in [9], which consumed more than double the mass of oxygen exhibited a burn exponent of 0.22. The same motor evaluated in this thesis operates with a burn exponent much larger, at 0.43. This is a reinforcement to the behavior of hybrid rock fuel regression, which says fuel regression is proportional to the amount of oxidizer flux injected through the port. As the oxidizer mass flux level decreased, the burn exponent increased flattening the curve, though by itself this does not make sense without the scaling factor. The scale factor for the large oxidizer flux motor was 0.112, nearly three times the magnitude of the low mass flux motor. Taking this into account, the regression rate for the low-mass flux motor was less than the previously observed large flux motor, which aligns with basic hybrid rocket theory.

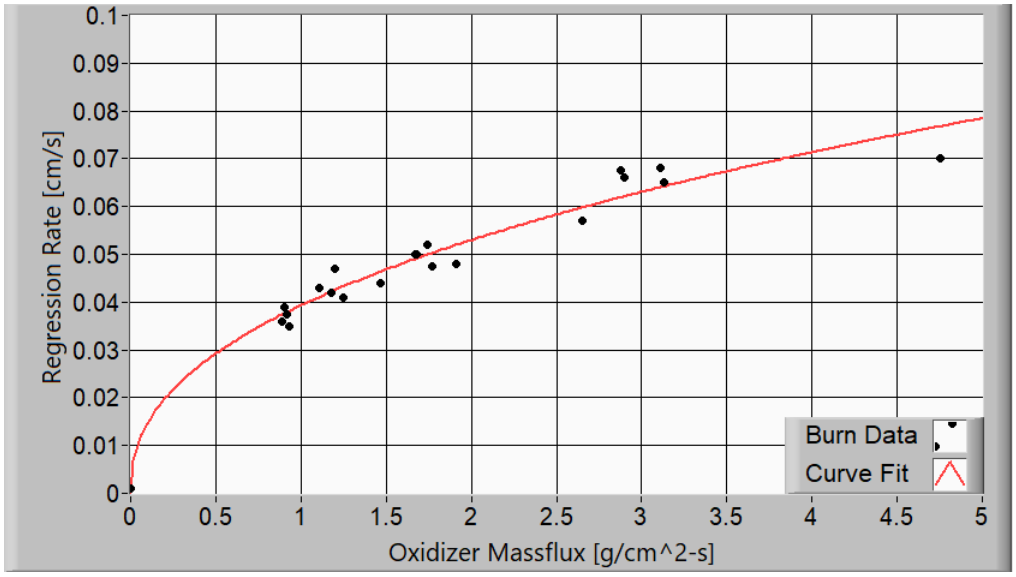

(a) GOX

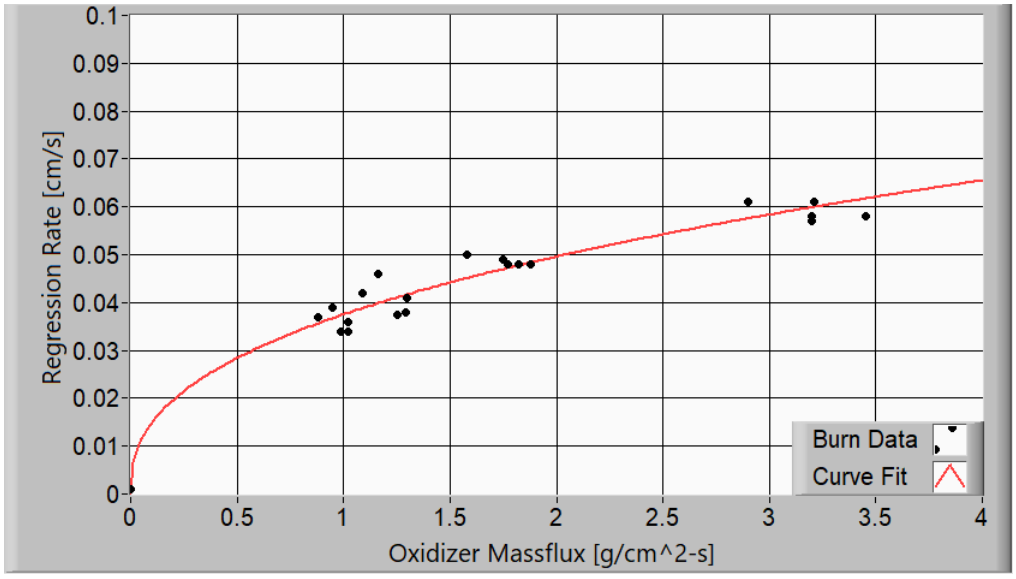

(b) 75%

Fig. 4.14: Regression vs Oxidizer Mass Flux

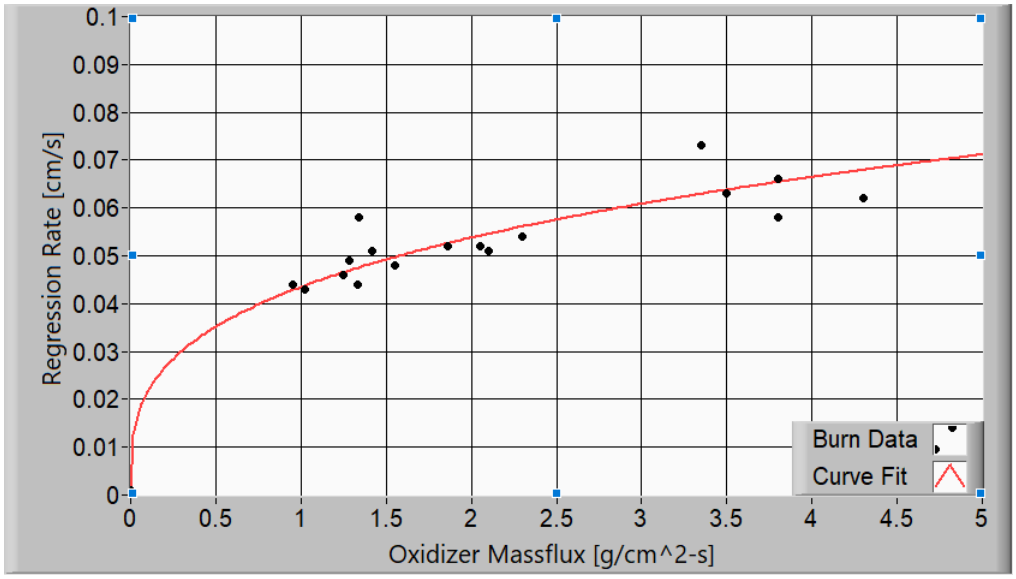

(a) 55%

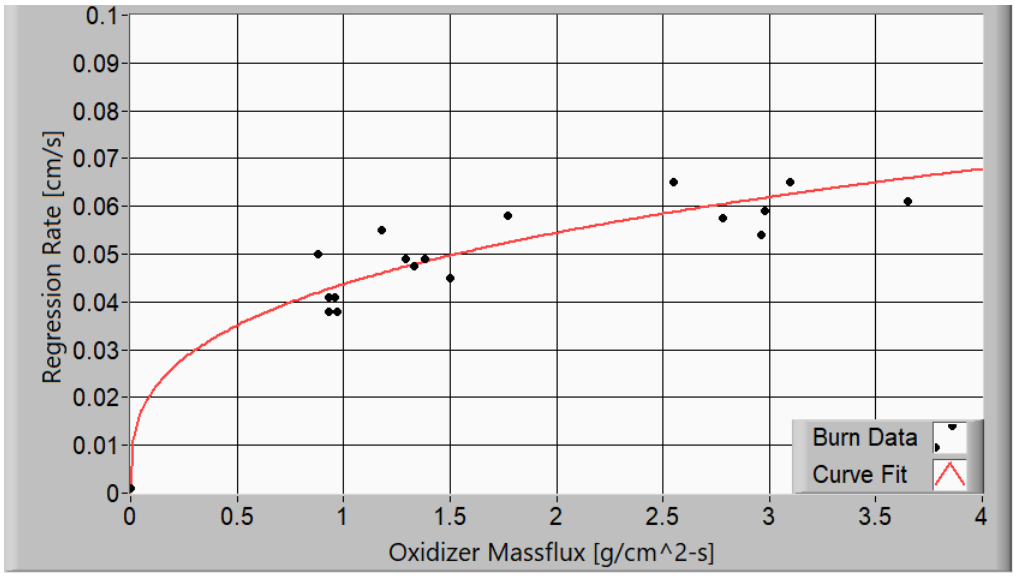

(b) EAN40

Fig. 4.15: Regression vs Oxidizer Mass Flux

The same results can be seen in Fig. 4.15, which plots the same regression data with the lower energy oxidizers, EAN40 and the oxidizer containing 55% oxygen. At first, the curves look nearly identical to Fig. 4.14. However, contrary to initial assumptions that

fuel regression would largely decrease with the low energy oxidizers, the fuel regression is actually larger after the oxidizer mass flux reaches approximately 1.25 $g/cm^2 - s$. For example, near end of life, the fuel grains actually burn with greater regression with EAN40, than with GOX. Explanation for this may lie in the physics surrounding hybrid rocket combustion, namely the friction model and Lee's blowing coefficient. Table 4.4 summarizes the fuel regression scale factors and burn exponents.

Table 4.4: Fuel Regression Scale Factor and Burn Exponent

Parameter	**a**	**n**
EAN40	0.044	0.32
55%	0.043	0.31
75%	0.038	0.40
GOX	0.039	0.43

CHAPTER 5

CONCLUSION

This thesis investigated the feasibility of replacing GOX with an industry recognized inert gas, an enriched air nitrox, for use as a hybrid rocket oxidizer. Testing originated as a response to an ongoing project known as USIP, where NASA awarded USU funding to fly a set of their prototype "green" hybrid thrusters on-board a NASA Sounding Rocket. Throughout the design process, the use of GOX was essentially blocked by NASA safety personnel; hence, the development phase of a moderately enriched compressed air began.

Initial tests evaluating burn characteristics of what is deemed EAN40 started in September of 2017. This testing was done on the first cut USIP design put forward by the senior design team, which proved to be difficult and time consuming due to the layout. Soon after these tests began, with growing demand for design documentation from NASA USIP personnel, all testing was ceased to design the flight unit previously shown in Fig. 3.1. By the time the new year came, the USIP deck was completed and ready for integration tests at the NASA Wallops Flight Facility. Soon after returning from these tests in early January 2018, motor evaluation resumed with multiple EAN40 tests. Approximately 58 fuel grains were burned between January 22nd, 2017 and March 2nd, 2017 with many injector, nozzle, and flow path modifications.

With plenty of data to analyze during the trip to Virginia for the flight demo in the middle of March, 2017, development of a LabVIEW analysis code began. This involved fine tuning the operating O/F ratios for CEA thermodynamic tables, developing routines to read the CEA output and the .csv files containing motor chamber and feed pressures, ignition voltage and current, and separate fuel mass measurements. The full analysis code used for the USIP 'dual' motor post-test analysis, along with the modified single motor post-test analysis evaluations at higher oxygen concentrations took nearly two months to fully qualify and compare to heritage analysis models. This was done as an independent

check to verify results and to gain further experience in working with large data sheets.

The flight data from the sub-orbital launch was not expected. Numerous ground tests qualified the ABS/EAN40 motor to perform consistently with regulated oxidizer feed pressures between 450 and 500 psia. During final integration and inspection, it was determined that the exposed pressure regulator was likely manipulated. A counterclockwise rotation of a few degrees would have decreased the feed pressure by tens of psi, impacting the motors ability to perform at expected levels. However, further evaluation led to the fact that the motor fuel grains became water soaked, then froze, during their 4+ day period of sitting on the launch rail. This water logged mode was the primary factor affecting motor performance, and was proven by a series of post launch ground tests with water soaked and frozen fuel grains. Section 4.2.4 describes these results in detail, identifying how the use of GOX would have immediately vaporized the water within the fuel grain. During peak motor performance, shown at the 15 second mark in Fig. 4.8, motor 1 specific impulse reached 200 seconds. A truly optimized nozzle for space applications would have produced a peak I_{sp} of 220 seconds.

The summary presented in Table 4.3 presents the results from a controlled, repeatable array of green hybrid thrusters tested at very low mass flux rates with four oxidizers: EAN40, 55% and 75% oxygen concentrations, and GOX. The chamber pressure remained within 5% of the target 250 psia for all tests. This target chamber pressure produced similar thrust levels regardless of the oxidizer choice, and was done to highlight the change in motor performance as the enthalpy of combustion decreased. The decrease in combustion energy between the highest and lowest energy oxidizer is a factor of ten, with EAN40's combustion enthalpy barely greater than the required energy to vaporize ABS fuel. Knowing this led to the surprising results of the fuel regression study, shown in Figs. 4.13 and 4.14, where the regression rate for EAN40 is slightly greater than GOX at low mass flux levels. Overall, while holding the chamber pressure constant, these results align with thruster predictions based on expected total exit mass flow rates, nozzle expansion ratio, and chamber pressure.

However, the model predictions based on ballistics modeling broke down and produced

unreliable results. Output from the ballistics model over-or-under predicted the chamber pressure, which yielded unstable fuel regression rates and specific impulse. The only true output from the ballistics model was the flow rate of oxidizer that was determined from a combination of unchoked and choked compressible mass flow equations, with its implementation depending on the conditions at the injector face. In the end, analytical predictions of motor performance was unreliable and has yet to be fully understood at these small scales.

CHAPTER 6

FUTURE WORKS

The results from this thesis indicate that a moderately enriched compressed air can function as a viable oxidizer for hybrid rockets. However, several areas surrounding this topic offer additional research endeavors.

Confusion regarding the ballistics of small scale hybrid rockets has yet to be understood. To better understand the modeling, controlled tests of several L/D ratio motors should be investigated, with the diameter remaining constant. Performing these tests with consistent oxidizer feed rates, chamber pressure, and nozzle geometry would be key in producing data sets for convenient correlation. During these tests, burn duration would be critical. As was seen in the regression study with the four oxidizers presented in this thesis, regression varies with oxidizer choice at low mass flux levels. This indicates that the varied L/D study would benefit from single burn duration tests consuming the majority of the fuel, and from tests with short pulsed burns. As the fuel grain port opens, the flux decreases, and the parameters controlling the ballistics model may require manipulation based on the boundary layer change within the port. This investigation would require a lot of testing with multiple fuel grains, however it could lead to a better understanding of why the ballistics model does not accurately predict motor performance at small scales and low L/D ratios.

The second research endeavor would be to discover the lowest, consistently attainable thrust level from a fully functional hybrid rocket. Small spacecraft typically require thrust levels at the sub-Newton level for precise attitude control, and all USU green hybrid thrusters have remained in the 4 N and above range. Regardless of exhaust plume characteristics, this study would prove out the possibility of hybrid rockets functioning as viable, green, and safe propulsion options for small spacecraft.

Lastly, less of a research endeavor and more of a desire, would be to gain another opportunity to fly these thrusters in a hard vacuum environment. The NASA USIP was

the first opportunity USU received to fly a set of small scale green hybrid thrusters on board a sub-orbital rocket. This led to inevitable design mistakes and communication hiccups between the USU senior design team and NASA. A second opportunity would lead a refined payload design, greater ability to work with NASA safety personnel in flying GOX, and likely lead to an examination with up to a dozen hot fire tests in a hard vacuum environment due to the advantageous rise time of GOX. However, in the end, the USU green hybrid thruster has gained flight heritage, unlike the previously discussed green propellant known as AF-M315E.

REFERENCES

[1] Asif Saddiqi, "The Man Behind the Curtain," *Air and Space Magazine*, pp. 1–4, 2007.

[2] M. V. F. Ribeiro and P. C. G. Junior, "Hybrid Rocket Motor Propellants: A Historical Approach," in *21st International Congress of Mechanical Engineering*, 2011.

[3] Pacific Rocket Society, "Loading and Launching of the XDF-3 Rocket," *Journal of the Pacific Rocket Society*, vol. 3, pp. 15–17, 1948.

[4] Shep Shepherd, "Fourth of July the Year Around," *Popular Mechanics*, vol. 101, no. 4, pp. 81–85, Apr 1954, Thiokol/LOX.

[5] Marxman and Gilbert, "Turbulent Boundary Layer Combustion in the Hybrid Rocket," in *Symposium on Combustion*, 1963, pp. 371–383.

[6] James Kennedy. (2014, July) How are Lego bricks made? The Chemistry of LEGO. Chemistry of Everything.

[7] P. Z. W. Whitmore Stephen A. and E. S. D., "Comparing Hydroxyl Terminated Polybutadiene and Acrylonitrile Butadiene Styrene as Hybrid Rocket Fuels," *Journal of Propulsion and Power*, vol. 29, no. 3, 2013.

[8] N. I. Stephen A. Whitmore and D. P. Merkley, "Development of a Power-Efficient, Restart-Capable Arc Ignitor for Hybrid Rockets," *Journal of Propulsion and Power*, vol. 31, no. 6, 2015.

[9] Whitmore Stephen. A. and M. A. B., "Vacuum Tests of a Novel Green Propellant Thruster for Small Spacecraft," *AIAA Paper 2017-5044*, 2017.

[10] Robert A. Braeunig. (2008) Rocket Propellants. online. Rocket and Space Technology. [Online]. Available: http://www.braeunig.us/space/propel.htm

[11] V. Bombelli and D. Simon, "Economic Benefits of the use of non-toxic mono-propellants for Spacecraft Applications," *AIAA Paper 2003-4783*, 2003.

[12] Iridium. (2017, June) Hydrazine - toxic for humans, but satellites love it. SpaceX/Iridium NEXT.

[13] William M. Marshall and M. C. Deans, "Recommended Figures of Merit for Green Monopropellants," *AIAA Journal*, 2013.

[14] Tracy McMahan. (2015, Sept) New Green Propellants complete Milestones. NASA. [Online]. Available: https://www.nasa.gov/centers/marshall/news/news/releases/2015/new-green-propellants-complete-milestones.html

[15] S. K. Rondald A. Spores, Robert Masse and C. McLean, "GPIM AF-M315E Propulsion System," *AIAA Paper 2014*, 2017.

[16] Stephen L. Merkley, "Effects of Radiation Heating on Additively Printed Hybrid Fuel Grain Oxidizer-to-Fuel Ratio Shift," Master's thesis, Utah State University, Logan, UT, 2016.

[17] Stephen A. Whitmore, "Additively Manufactured Acrylonitrile-Butadiene-Styrene Nitrous-Oxide Hybrid Rocket Motor with Electrostatic Ignitor," *Journal of Propulsion and Power*, vol. 31, no. 4, 2015.

[18] Whitmore Stephen. A. and M. D. P., "Arc-Ignition of a 70%-85% Hydrogen Peroxide/ABS Hybrid Rocket System," *AIAA Paper 2017-5017*, 2017.

[19] R. J. Muzzy, "Schlieren and Shadowgraph Studies of Hybrid Boundarylayer Combustion," *AIAA Journal*, vol. 1, no. 9, pp. 2159–2160, 1963.

[20] Elizabeth T. Jens, "Hybrid Rocket Combustion And Applications To Space Exploration Missions," Master's thesis, Stanford University, Stanford, CA, 2015.

[21] George P Sutton and O. Biblarz, *Rocket Propulsion Elements*, 9th ed. Wiley, 2013, iSBN: 978-1118753658.

[22] John D. Anderson, *Modern Compressible Flow with Historical Perspective*, 3rd ed. McGraw-Hill Education, 2002, iSBN: 978-0072424430.

[23] Joel H. Marshall, "Thrust Augmented Nozzle For A Hybrid Rocket With A Helical Fuel Port," Master's thesis, Utah State University, Logan, UT, 2017.

APPENDICES

APPENDIX A

NASA USIP Fill Procedure

THIS LOCAL PROCEDURE/WORK INSTRUCTION CONTAINS HAZARDOUS OPERATIONS

LOCAL PROCEDURE/WORK INSTRUCTION UTAH-PRESS-001

UTAH STATE UNIVERSITY FILLING PROCEDURE

Document Owner:

Rev - Official Release Date: 02/26/2018

Safety Cover page

1.0 Purpose:

The purpose of this document is to outline the basics of pressurizing and depressurizing Utah State University pressure vessels.

This procedure describes instructions for:

1) Filling flight vessels

2.0 Scope: This document covers the fill procedure of either installed or free 13 cu. in. HPA (3000 psig) flight vessels only

3.0 Definitions/Acronyms:

HPA – High Pressure Air
EAN – Enriched Air Nitrox
EH&S – Environmental, Health, and Safety Office
USU – Utah State University
Source Tank – large volume high pressure tank used to fill flight vessel
Flight Vessel – low volume flight tank

4.0 Resource Requirements:

- Safety specialist for oversight of filling operation

5.0 Equipment Requirements:

The following equipment is required as a minimum (items marked *italic* are to be provided by NSROC):

- Source tanks containing desired gas
- Source tanks with Certified regulator/gage set-up
- Fill line rated for filling pressure
- Wrenches
- Fill tank with appropriate connections
- Safety glasses

6.0 Training Requirements:

- The Operations Safety Specialist (OSS) must be familiar with the pressure systems and/or be thoroughly briefed prior to operations.
- The operator must have a working knowledge of the pressure systems.
- All personnel working with high pressure systems shall be thoroughly familiar with the hazards involved as defined in GPR 8719.17A. They shall also be familiar with all emergency measures that may be required in the

event of an accident. Any contractor organization that has an equivalent training program may be equivalently certified to these training requirements with approval of the WFF Safety Office.

7.0 Safety Requirements:

NOTE: This procedure contains operations which are considered hazardous, and thus requires an OSS in addition to the system operator. The OSS must be an independent observer and shall not perform or assist in the performance of any hazardous operation.

Personnel working in the area should be informed that hazardous pressure operations are going to be conducted. The payload shall be oriented such that, if a fast vent or bottle rupture were to occur, the output will not injure personnel.

Note: During the hazardous portions of the operation, only personnel directly involved with the hazardous portions of the operation are permitted access to the payload and must wear the proper PPE.

7.1 For multiple operations, no hazard areas will be permitted to overlap each other.

7.2 Prior to beginning a hazardous operation, the OSS shall define a hazard area that will contain all components of the article during assembly, including liquid spills

7.3 Under direction of the OSS, the hazard area shall be cleared of nonessential personnel prior to beginning of pressurization operations. The defined hazard area must consider all possible contingencies that may lead to inadvertent projectiles and shall make an announcement that a hazardous operation is about to commence.

7.4 Any facility where personnel may inadvertently enter a hazard area must be clearly identified prior to beginning pressure/cryogenic operations. Door identification shall prevent personnel from entering the hazard area while permitting personnel to exit at any given time.

7.5 If a hazardous operation is being performed, the OSS or operator doing the operation shall conduct a safety briefing prior to any operation being performed. The briefing will include all essential personnel involved in the hazardous operation. The briefing shall cover all details of the operation, specify procedures to be used, and ensure clear understanding of the hazardous operation about to be performed and hazards involved.

7.6 Once the procedure is completed and the hazard is safeguarded, the technician and the OSS shall indicate an “All Clear” status that the article is now in the safe condition.

7.7 All completed procedures must be collected and reviewed by the OSS for safety deviation.

8.0 References:

- GPR 8719.17A
- WFF Range Safety Manual (RSM)-2002 Rev C (use Current Rev)

9.0 Quality Assurance:

9.1 All operators participating will print their name below and initial beside their name.

_____	_____	_____	_____
Printed Name	Initials/Date	Printed Name	Initials/Date
_____	_____	_____	_____
Printed Name	Initials/Date	Printed Name	Initials/Date

Identify OSS for this work instruction.

_____ _____
Printed Name Initials/Date

9.2 Operator will verify that the required procedural steps are accurately performed and complete. To attest that this has been accomplished the operator will initial and date each sign-off indicating satisfactory completion of each step as performed.

9.3 Each step shall be signed prior to proceeding to the next step. If it is necessary to perform steps out-of-order, a red line shall be added to the work instruction identifying the steps that were performed out-of-order and the reason for the deviation. Prior to proceeding with the re-sequenced steps, concurrence from the principal investigator (PI) and OSS and mission manager must be obtained. If the performed-out-of-order steps are within a section requiring an OSS, OSS approval (initials) of the red line is required prior to proceeding. If the performed-out-of-order steps are in a section that does not require an OSS, the PI, or the mission manager must approve (initial) the red-line prior to proceeding. For the non-hazardous section, the OSS can approve the red-line later.

9.4 If a task is stopped prior to completing the section describing that task, the time, date, and nature of the stoppage (lightning, lack of parts, etc.) shall be noted on the bottom of the step where the stoppage occurred. A note at the bottom of the page shall also describe any steps that were required to put the system into a SAFE condition and any other pertinent information.

9.5 Upon re-starting the stopped operation, another note shall be generated indicating when the operation resumed, and the safety precautions performed prior to re-starting the task. Examples of these precautions include (but are not limited to) checkout of GSE, verification of proper PPE, clearance of danger areas, and hazardous operations briefing.

9.6 If the work stoppage was in a section requiring an OSS, the OSS must initial the notes describing the nature of the work stoppage and note before starting a stopped operation.

9.7 After completing each section, the technician will sign indicating satisfactory completion of each section. If an OSS was required for the section, the OSS shall also sign at the end of the section indicating successful completion of the section.

9.8 Participating personnel (technicians and/or OSS's) are encouraged to note any pertinent information in notes section on the bottom of section 10.0 pages. If additional space is required, the margins or backs of pages can also be used for notes.

10.0 Implementation: FILLING TANKS

10.1 Title of Step
(Hazardous, OSS Required)

WARNING: Operator, throughout operation should monitor vents, valves, etc. to anticipate and avoid possibility of a rupture of the test article.

10.1.1 ***Be sure that all cylinders to be filled have a current, valid hydrostatic test date. Verify maximum fill pressure.***

10.1.2 Confirm OSS HAZOP briefing has been performed

10.1.3 Ensure the source tanks being used are secured

_____ _____
OSS/DATE OPERATOR/DATE

10.1.4 Connect the source tank, via the fill line/quick disconnect to the flight vessel

_____ _____
OSS/DATE OPERATOR/DATE

10.1.5 Before opening the source tank valve, fully close the flight vessel inlet valves

10.1.6 . Fully open the source tank

10.1.7 **Slowly** open the flight vessel inlet valve to pressurize (adjust fill adapter nozzle to provide a fill rate of 100 psig/second)

10.1.8 Once the system reaches pressure equilibrium, close source tank outlet valve

10.1.9 Close flight vessel inlet valve

_____ _____
OSS/DATE OPERATOR/DATE

10.1.10 Bleed off the residual pressure in the fill hose by slowly opening the silver bleeder valve identified in the diagrams below

10.1.11 Disconnect the fill line from the pressurized flight vessel

10.1.12 Certification that section 10.1 of this procedure has been completed.

_____ _____
OSS/DATE OPERATOR/DATE

Emergency Back-out Procedure:

10.2 Title of Step
(Hazardous, OSS Required)

WARNING: Operator, throughout operation should monitor vents, valves, etc. to anticipate and avoid possibility of a rupture of the test article.

10.2.1 ***If procedure is interrupted due to any malfunction of tank, valve, or line, follow the steps below.***

10.2.2 Immediately close both the source and flight vessel

10.2.3 If the fill line is pressurized, depressurize by opening bleed valve

10.2.4 Close bleed valve

10.2.5 Disconnect the fill line from the flight vessel

10.2.6 Ensure the flight vessel regulator is securely fastened to the vessel

10.2.7 Ensure universal fill adapter is securely fastened to flight vessel regulator

10.2.8 Ensure fill whip connection is securely mounted to source tank

10.2.9 Re-connect the quick-disconnect to the flight vessel

10.2.10 Go to fill procedure and follow the steps listed there

10.2.11 If this does not work, equipment may be broken: Contact equipment specialist

Diagrams:

Part	Relief Valve Set Pressure	Work Pressure [psi]	Max Pressure [psi]	Temperature Rating	Cool down/Warm Up Rate	Pressure Vessel Requirements	Cleaning Requirements	Pressure Protection for Vacuum Vessel	Thermal Stress Analysis
Source Tank -- Kaplan Scuba Tank	N/A	3000	5000	[0C˚-50C˚]	N/A	Fill whip/fill line/quick disconnect	N/A	N/A	N/A
Taousa 70231 Scuba Fill Station	N/A	4500	Unknown	Unknown	N/A	N/A	N/A	N/A	N/A
First Strike HERO 4.5K Regulator	1.8kpsi & 5kpsi	4500	Unknown	Unknown	N/A	N/A	N/A	N/A	N/A
Ninja - Universal Fill Adapter	N/A	4500	Unknown	Unknown	N/A	N/A	N/A	N/A	N/A
First Strike 3k Pressure Vessel	N/A	3000	5000	Unknown	N/A	Regulator/Fill Adapter	N/A	N/A	N/A

Figure 1: Component Specifications

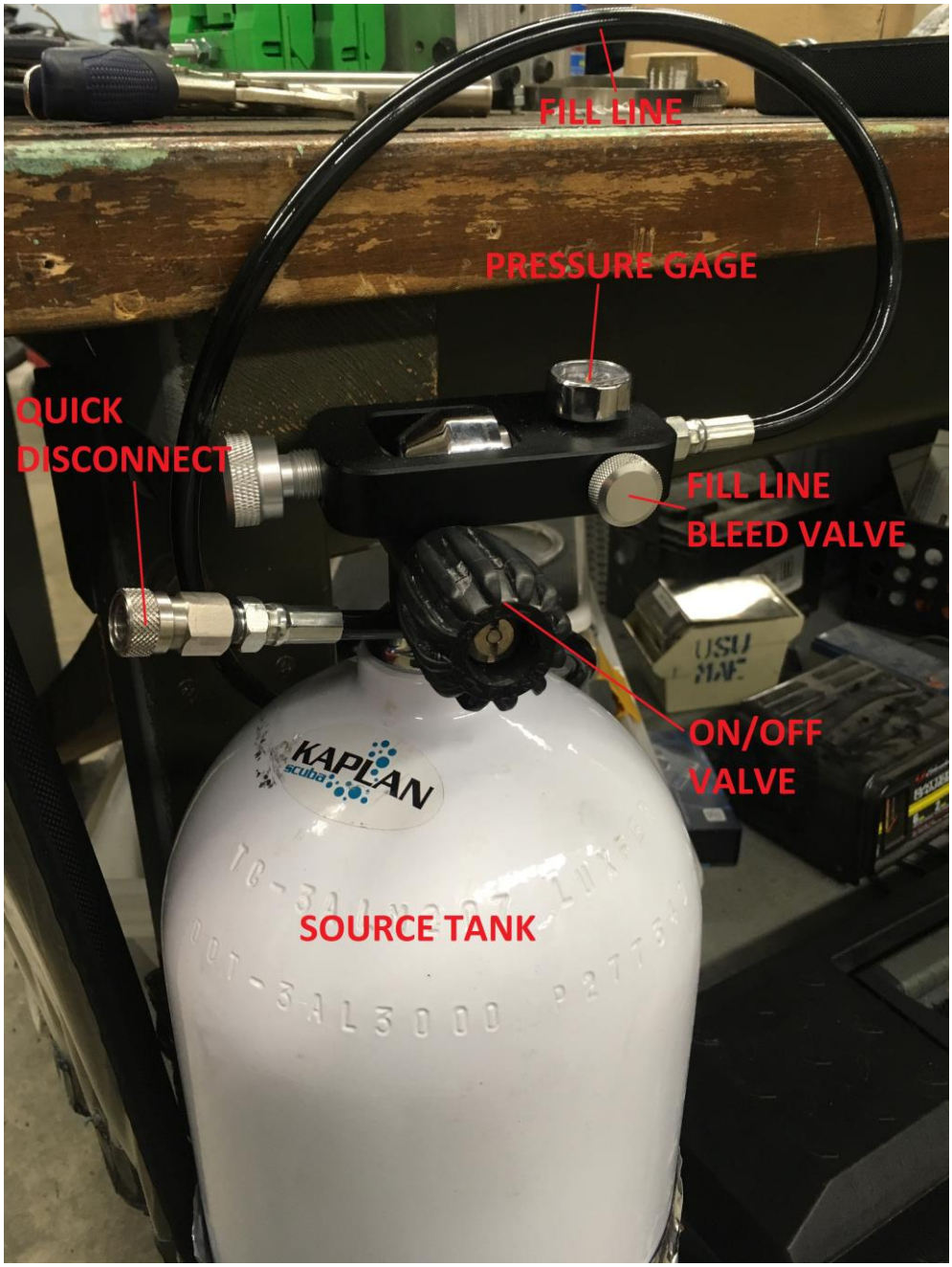

Figure 2a: Source Tank Explained

Figure 2b: Flight Vessels Explained

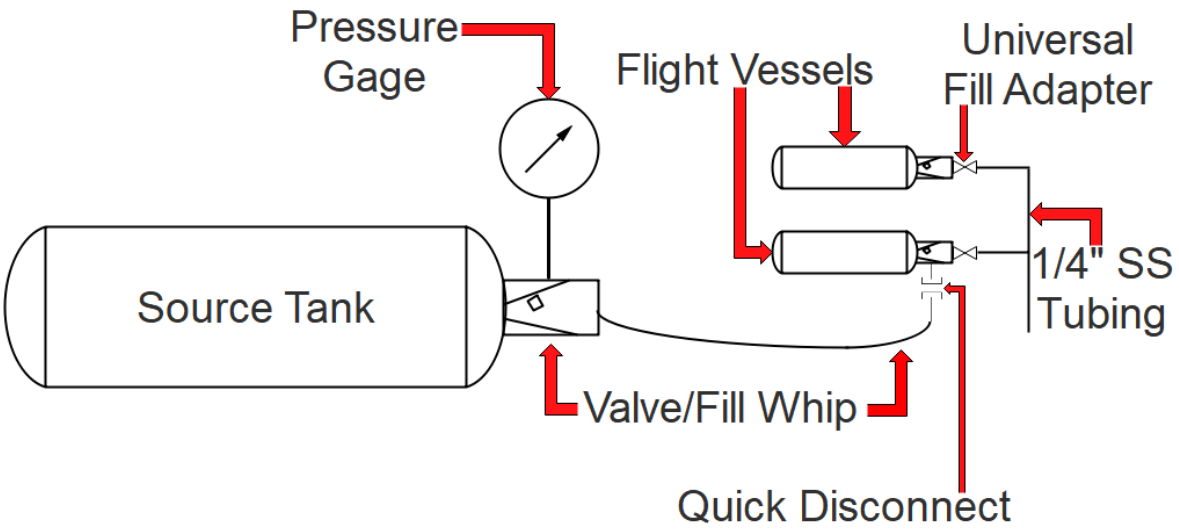

Figure 3: Plumbing Diagram of Fill Station

11. Quality Records:

Quality Records are controlled in accordance with NSROC Procedure QS44161. A master list of QMS quality records is maintained by CM and is referenced in QS44161. Quality Records for this process are noted below along with specific file locations. Unless otherwise noted, the retention time will be 3 years after delivery of all items and/or completion of all services called for by the contract.

Record	File Location

REVISION CONTROL PAGE

Revision	Effective Date	Description of Change
Rev -		Establish Baseline